

Geometries of Light

by

Ramon Elias Weber

Bachelor of Science ETH in Architecture,
Swiss Federal Institute of Technology Zurich (2016)

Master of Science, University of Stuttgart (2018)

Submitted to the Program in Media Arts and Sciences, School of Architecture and
Planning, in partial fulfillment of the requirements for the degree of Master of Science in
Media Arts and Sciences

at the

Massachusetts Institute of Technology

May 2020

© Massachusetts Institute of Technology, 2020. All rights reserved.

Author

.....

Ramon Elias Weber

Program in Media Arts and Sciences

May 11, 2020

Certified by

.....

Neri Oxman

Associate Professor of Media Arts and Sciences

Accepted by

.....

Tod Machover

Academic Head, Program in Media Arts and Sciences

Geometries of Light

by

Ramon Elias Weber

Submitted to the Program in Media Arts and Sciences, School of Architecture and Planning, on May 8, 2020 in partial fulfillment of the requirements for the degree of

Master of Science in Media Arts and Sciences

Abstract:

This research aims to create architectural geometries that are driven by performance — in light, energy, and structure. Given a new relationship between building matter and environment, built artefacts and envelopes no longer act as passive shells, but actively shape and interact with their surroundings. Our built environment is one of the main contributors to climate change. Tackling this global challenge requires rethinking current design methodologies and workflows. How can we create buildings of the future that work together with their environment and embody a new design paradigm where architectural geometry works together with the forces of nature, using material and light as design drivers?

Proposing a new design framework for the human habitat, this thesis investigates building envelopes of the future. For this, photon mapping is evaluated as an advanced lighting simulation method for optically complex structures on an architectural scale. We investigate workflows driven by artificial intelligence (AI) to open new ways for design space exploration and generation that map geometric data to light behavior. Furthermore, we see how building scale illuminance and structural performance can be combined to unlock design potential and create a new architectural vocabulary.

Thesis advisor:

Neri Oxman

Associate Professor of Media Arts and Sciences

Geometries of Light

by

Ramon Elias Weber

This dissertation/thesis has been reviewed and approved by the following committee members

Neri Oxman

.....

Associate Professor of Media Arts and Sciences

School of Architecture and Planning

Caitlin Mueller

.....

Associate Professor in Building Technology

School of Architecture and Planning

Christoph Reinhart

.....

Professor in Building Technology

School of Architecture and Planning

Acknowledgments

My deepest gratitude goes out to my advisor Neri Oxman for her mentorship and guidance at MIT and beyond. I want to thank my co-advisors Caitlin Mueller and Christoph Reinhart for the inspiring conversations and directions that lead my research deep into building science. I want to thank the whole Mediated Matter Group for the warm home at the Media Lab, the inspiring teamwork and the truly interdisciplinary thinking around algorithms, ecosystems and fabrication: Joe Kennedy, Felix Kraemer, Jean Disset, Christoph Bader, Sunanda Sharma, James Weaver, Rachel Soo Hoo Smith, Nic Lee, Susan Williams, Josh Van Zack, Ren Ri, João Costa, Jorge Duro-Royo, Becca Bly, Kelly Egerova and Natalia Casas. Michael Stern I especially thank for his input on the Glass 3D printing process and Peter Houk and the team at the MIT Glass Lab for the introduction to glassblowing.

Furthermore, I would like to thank Tom Lutz for his help with the 3D scanning, Yijang Huang and Renaud Danhaive for their inputs and advice on the computational methods, Dr. Roland Schregle and Dr. Lars Grobe for their valuable help and initial discussions around photon mapping and Dan Weissman for his advice on the artificial lighting experiments. I would like to thank Lukas Debiase, Nitzan Zilberman, Zach Cohen, Nof Nathanson and Christophe Guberan for all the inspiring discussions around my work.

I want to thank Philippe Block for all the years of inspiration and guidance, leading me into the world of architectural research and eventually to MIT. With tears in my eyes a special thank you goes to Matthias Rippmann for his friendship, challenging, teaching and believing in me.

A thank you goes to my former advisors and mentors at the University of Stuttgart; Achim Menges and Jan Knippers, and at Zaha Hadid Architects in London; Patrik Schumacher, Shajay Bhooshan, Nils Fischer and Cristiano Ceccato for shaping my thinking around architecture and design.

Finally, I would like to thank my parents Sandra Beriger and Rainer Weber and my brother Yannick Weber for all their love, encouragement and support and making me believe in the impossible.

Contents

1	Introduction.....	13
2	Background.....	15
3	Photon Mapping of Geometrically Complex Glass Structures: Methods and Experimental Evaluation.....	18
3.1	Abstract	18
3.2	Introduction.....	18
3.3	Methodology	23
3.3.1	Validation Experiments.....	23
3.3.2	Experimental Setup A: Interior Lighting	24
3.3.3	Experimental Setup B: Exterior Lighting.....	24
3.3.4	Geometry Workflow	26
3.3.5	Digital Simulation.....	27
3.4	Results	28
3.4.1	Results of Experiment A: Indoor Lighting.....	29
3.4.2	Results of Experiment B: Exterior Lighting.....	32
3.5	Discussion	34
3.5.1	Geometric Detail.....	35
3.5.2	Simulation Parameter Settings	36
3.5.3	Opportunities for Design.....	37
3.6	Conclusion.....	37
4	Programmable Caustics.....	39
4.1	Introduction.....	39
4.2	Methods.....	39
4.2.1	Modeling of Simplified Design Space	39
4.2.2	Geometry Constraints of Additively Manufactured Glass	40
4.2.3	Parametrization of Printable Geometry.....	42
4.2.4	Neural Network Creation	44
4.3	Results	45
4.4	Discussion	47
4.4.1	Sources of Error	47
4.4.2	Contributions.....	47
4.5	Outlook.....	48
4.5.1	Further Neural Net Development	48
4.5.2	Design Implications	48

5	Structural Shading	50
5.1	Abstract	50
5.2	Introduction	51
5.3	Methodology	53
5.3.1	Design and Optimization Workflow	54
5.3.2	Methods for Structural Optimization	56
5.3.3	Methods for Environmental Analysis	57
5.4	Results	58
5.4.1	Experiment A: Adaptive Materiality for Lower Embodied Energy	58
5.4.2	Experiment B: Material Optimization for Solar Radiation	60
5.4.3	Experiment C: Geometry Optimization for Solar Radiation	61
5.4.4	Experiment D: Seasonal Optimization for Facades	61
5.5	Discussion	63
5.6	Conclusion	64
6	Conclusion.....	70
7	References	73
8	Appendix	81
8.1	Neural Net definitions	81
8.1.1	NN1	81
8.1.2	NN2	82
8.1.3	NN3	83

List of Figures

Figure 1: Light behavior in the real world 1-3. as compared with traditional digital simulation methods 4-6 and the photon mapping approach 7-8.	16
Figure 2: Geometrical complexity in a glazed building envelope, King Abdullah Financial District Metro Station in Riyadh, designed by Zaha Hadid Architects. Exterior rendering (left), construction of façade diagrid (middle, photograph by Faisal Bin Zarah) and close-up of detailed facade mockup (right) (all images property of RDA and courtesy of ZHA).....	20
Figure 3: Additive manufacturing of optically transparent glass by the Mediated Matter Group, MIT Media Lab. Glass object with caustic pattern (top left), 3D printing process (top right), variety of printable objects (bottom left) and glass column with inserted light (bottom right) (all images courtesy of the Mediated Matter Group).	21
Figure 4: Schematics of experimental setups A and B with 3D printed glass object (1), digital camera (2) and luminance meter (3). Experiment A is set up in an indoor environment with the artificial light source, Sora Par20 10.8W (4). Experiment B is conducted in a closed box (6) in an outdoor environment.	25
Figure 5: Photographs of physical setup of experiment B with interior view of lit cylinder (left). An exterior view of the 3D printed glass cylinder in sunlight (middle) and the measurement via digital camera, Canon EOS 5d Mark III and the Konica Minolta LS-110 luminance meter (right).....	26
Figure 6: Remodeling workflow for 3D printed glass. A sample geometry is scanned and mapped onto a final geometry to create the mesh used in the lighting simulations (A-E).....	27
Figure 7: Comparison of HDR photograph and Radiance photon map simulation of no object (test 0), cylindrical tube (test 1), three bulges (test 2) and four bulges (test 3).	30
Figure 8: Plots of brightness values (left) with measured and simulated luminance in logarithmic scale and a smoothened, scaled and capped overlay of both datasets in linear scale with the resulting root mean square error. Image split (right) shows an HDR photograph overlaid on the digital simulation with a red line indicating the position of the luminance measurements in the plots.	31
Figure 9: 3D printed glass cylindrical tube in daylight captured as false color HDR photographs and <i>Radiance</i> photon mapping simulations.	33
Figure 10: Light level comparison, Cd/m ² , of a fixed point inside the box in Experiment B of both digital Radiance simulation and physical measurements. A sample image of the digital Radiance simulation at 9:30 am is depicted (top right corner). The red square indicates the area of where the luminance value average was measured. A visual glare threshold of > 2000 Cd/m ² is displayed in yellow.	34
Figure 11: Sources of error through low resolution mesh representation for the number of photons scattered in the scene. A low-resolution mesh (a) with 4915 faces is compared with a high-resolution mesh (b) with 370252 faces.	36
Figure 12: Photon maps (left to right) with 10000 photons, 200000 photons and 10000000 photons increase the resolution and accuracy of the caustic simulation.	36
Figure 13: Comparison in falsecolor scale of HDR photograph (left) and Radiance photon map simulation (right).	38

Figure 14: Setup of minimal raytracer to evaluate lenses where light rays are projected from an emitter surface through the lens and captured by an image plane.....	40
Figure 15: Design space exploration of lens geometry and their corresponding caustic pattern.....	40
Figure 16: Parametric fabrication-aware boundary creation and extrusion workflow for the source glass geometries.....	41
Figure 17: Creation of caustic photon map with raytracing through parametric glass geometry	42
Figure 18: Selection of 40 out of 5,000 resulting caustic maps	43
Figure 19: Geometry to caustic to neural net pipeline	44
Figure 20: Input images (top row) were processed by the neural net. Output images (bottom row) resulting from the predicted geometry parameters.....	45
Figure 21: Input shapes (top two rows) with corresponding caustic image and output geometries (bottom two rows) with corresponding caustic images.....	46
Figure 22: Abstract input caustic images (top row) and the processed output caustic maps based on the predicted geometry vector.....	46
Figure 23: Closeup of photon map with 10'000 scattered points.....	49
Figure 24: Architectural typologies tested in the digital experiments: Freestanding roof (1.), gridshell with two open sides (2.), gridshell façade (3.).	53
Figure 25: Description of digital experiments A-D with their setup, variables and optimization parameters.	54
Figure 26: Overview diagram for iterative computational design workflow, utilizing structural and environmental performance for multi-objective optimization.	55
Figure 27: Level set method for adaptive material selection.	56
Figure 28: Degree day selection, as adapted from Reinhart (C. Reinhart 2014) for Boston: April 25th, ordinal date (od) 115, to October 21st, od 294, summer solstice June 20th, od 172.....	57
Figure 29: Cross-section selection range in relation to the weight of the overall structure.....	58
Figure 30: Visualizations of input for structural simulation as fixed mesh with four supports, materialization in timber (a1.) with failing cross sections in red, and all-steel solution (a2.), final material combination (a3.)......	59
Figure 31: Sampling of design space with visualized weight and embodied energy of solutions.....	60
Figure 32: Material optimization towards a shading goal: Maximum shading (b1.), minimum shading (b2.) and area selective shading (b3.).	60
Figure 33: Geometric variation is achieved through the vertical movement of control points. Optimized mesh for maximum shading on the left sensor surface (c1.) and the right sensor surface (c2.).	61
Figure 34: Façade optimization setup: Definition of loads and supports (1.), core (2.), diagrid (3.), rotation of beams (4.), dimensioning of beams (5.) and simulation of illuminance and solar radiation (6.).	62
Figure 35: Sample façade iterations in elevation and closeup renderings at winter and summer solstices.	63

Figure 36: Summer and winter solstice daily average of luminance levels and embodied energy. The summer winter variance is the result of equation (1). Reference values were obtained by analysing the sensor surface without obstructing building geometry.	63
Figure 37: Interior rendering of iteration d1 with the façade letting light through at the winter solstice at 11:00 am.	65
Figure 38: Interior rendering of iteration d1 with the façade blocking light at 11:00 am.	65
Figure 39: Rendering of the Structural Shading design framework applied to a façade geometry	67
Figure 40: Rendering of the Structural Shading design framework applied to a façade geometry	68
Figure 41: Rendering of the Structural Shading design framework applied to a façade geometry	69
Figure 42: Relationship between physical and digital geometry during the proposed manufacturing process.	71

List of Tables

Table 1: Comparison of 3D printed glass objects used in validation experiments.....	23
Table 2: Sample commands for the photon mapping approach (variable files indicated with {file})..	28
Table 3: Radiance material definitions of the 3D printed glass material (Glass) and the box interior material (White).....	28
Table 4: Material definitions used in the structural simulation.....	56

1 Introduction

As simulation tools for light and energy produce more accurate reflections of our real world, and artificial intelligence (AI) and generative design environments allow for a virtual evolution of objects and spaces, the digital and physical domains come closer together. New abilities in additive manufacturing and digital fabrication at the building scale allow for unparalleled geometric freedom and resolution in the design of architectural structures. These advances in material research, manufacturing machinery, and design methods enable geometric complexity and accurate virtual-to-real-world prediction of their properties, without added cost. This thesis will investigate how this newfound material complexity can be combined with computational design strategies towards the creation of novel, performative design solutions.

New manufacturing tools and design environments require rethinking geometric creation and representation. Established modes of drawing during design stages have to be expanded to leverage computational intelligence. In this thesis, we will explore different layers of resolution that are needed for different stages of the design process. We can distinguish between geometry used for design, geometry used for fabrication, geometry used for analysis, and the actual physical geometry of an object. We can identify intricate relationships and feedback loops between them to understand their relationships throughout different stages of design.

Generative and parametric tools allow us to create almost infinite loops and variability in our creations. This results in an overflow of information that poses new challenges to designers and decision-makers. New methods of data visualization and the creation of design-specific metrics can help us to navigate complex design spaces. Different modes of abstractions on higher levels further allow us to truly take advantage of these design tools.

Specifically, the work aims to develop new experimental methods for design exploration and generation using generative and AI-driven design workflows to create performative design solutions on the building scale. Creating integrative design workflows that include environmental performance metrics such as daylight as well as structural considerations and embodied energy.

The thesis will focus on the digital design and implementation of novel workflows for use with existing source materials and fabrication platforms. Investigation of the creation of novel materials for additive manufacturing or the creation of new manufacturing machinery is outside of the present scope.

The first chapter, *Photon Mapping of Geometrically Complex Glass Structures*, dives into the relationship of the physical and digital. 3D printing of optically transparent glass by the Mediated Matter Group at the MIT Media Lab showcased the creation of highly complex objects that could be further developed towards large scale applications in the built environment. It was observed that the behavior of light, when scattered through complex transparent materials, cannot be simulated with conventional methods. We use the novel glass 3D printing system to benchmark and evaluate the photon mapping approach for the prediction of light levels and caustic patterns. Using data pairs of physical measurements and digital simulations, we can assess our computational strategies. The high geometric complexity of the 3D printed glass objects allows us to validate our findings across scales and creates the opportunity for architectural components to be developed as a new tectonic system on a building scale.

In the second chapter, *Programmable Caustics*, we approach light from a generative perspective. By creating geometry through a parametric workflow, we are able to iterate through tens of thousands of refractive geometries. We explore how geometric data and light behavior can be mapped through large datasets and propose that machine learning algorithms with convolutional neural nets can be used to navigate complex design spaces. Tailoring the geometric creation to existing image recognition algorithms, high-resolution lightmaps are mapped to low-resolution bitmap datasets, and in an inverse design process, light behavior becomes the starting point of the design.

The third chapter, *Structural Shading*, changes the scale of light simulation and focuses on building scale illuminance performance with shading systems. A design workflow for the creation of structurally performative shading envelopes is proposed. The creation of multifunctional building components is achieved through the combination of parametric geometry workflows, light simulation, and structural analysis tools. We demonstrate the importance of fabrication-aware simulation and show the impact of architectural material choices and geometry on embodied energy and environmental performance of structures across typologies.

2 Background

With current developments in additive manufacturing, architectural scale applications of highly complex non-standard building components are becoming more and more feasible. A number of large-scale experimental projects such as a 3D printed facade of Polyethylene Terephthalate Glycol-modified (PETG) polymer in Munich (Hemming-Xavier and Ostermaier 2019) and a large-scale 3D printed metal bridge (Block 2018) provide an outlook for future developments. Furthermore, a series of slabs, fully 3D printed in sand (Rippmann et al. 2018) or constructed using the 3D printed components as lost formwork (Jipa et al. 2019; Meibodi et al. 2018; Ruffray et al. 2017) show how additive manufacturing can be integrated into real-world construction projects. The geometric freedom unlocked by additive manufacturing of components can be leveraged to create structures that are lighter and only use material where needed, such as the metal structural nodes by Arup (Galjaard, Hofman, and Ren 2015). In the case of metal, even though multiple functionalities can be integrated into a single 3D printed element (Sarat 2018), the high price for additive manufacturing makes it impractical for the construction of buildings and only relevant for high-performance use in aerospace or very specialized industries.

Out of the research on additive manufacturing of optically transparent glass in the Mediated Matter Group came a manufacturing platform for the fabrication of large-scale components. The extrusion-based printing of glass enables the specification of geometry and surface structure of glass components using computer-aided design (CAD) models (Klein et al. 2015). The optical clarity creates highly complex caustic patterns when light is projected through a printed object. The curvature and surface texture, as striations or bulges visible layering of the 3D printed surfaces, allow for a high degree of control of the reflection, redirection, and shading of light passing through the transparent surface. The consistency and control of the fabrication parameters furthermore allow for a direct relationship between a light source and the caustic reflection, creating the potential for inverse design of the geometry through the control and definition of the light's behavior.

To control the relationship of glass with its environment — more specifically, the light passing through — a system for the computational simulation of caustic reflections and refractions had to be developed. In this thesis, the rendering platform, *Radiance* (Ward, G. and Shakespeare 1998), with its photon mapping extension (R. Schregle, Grobe, and Wittkopf 2016), was used and experimentally validated for the prediction of light behaviors through highly complex 3D printed glass components.

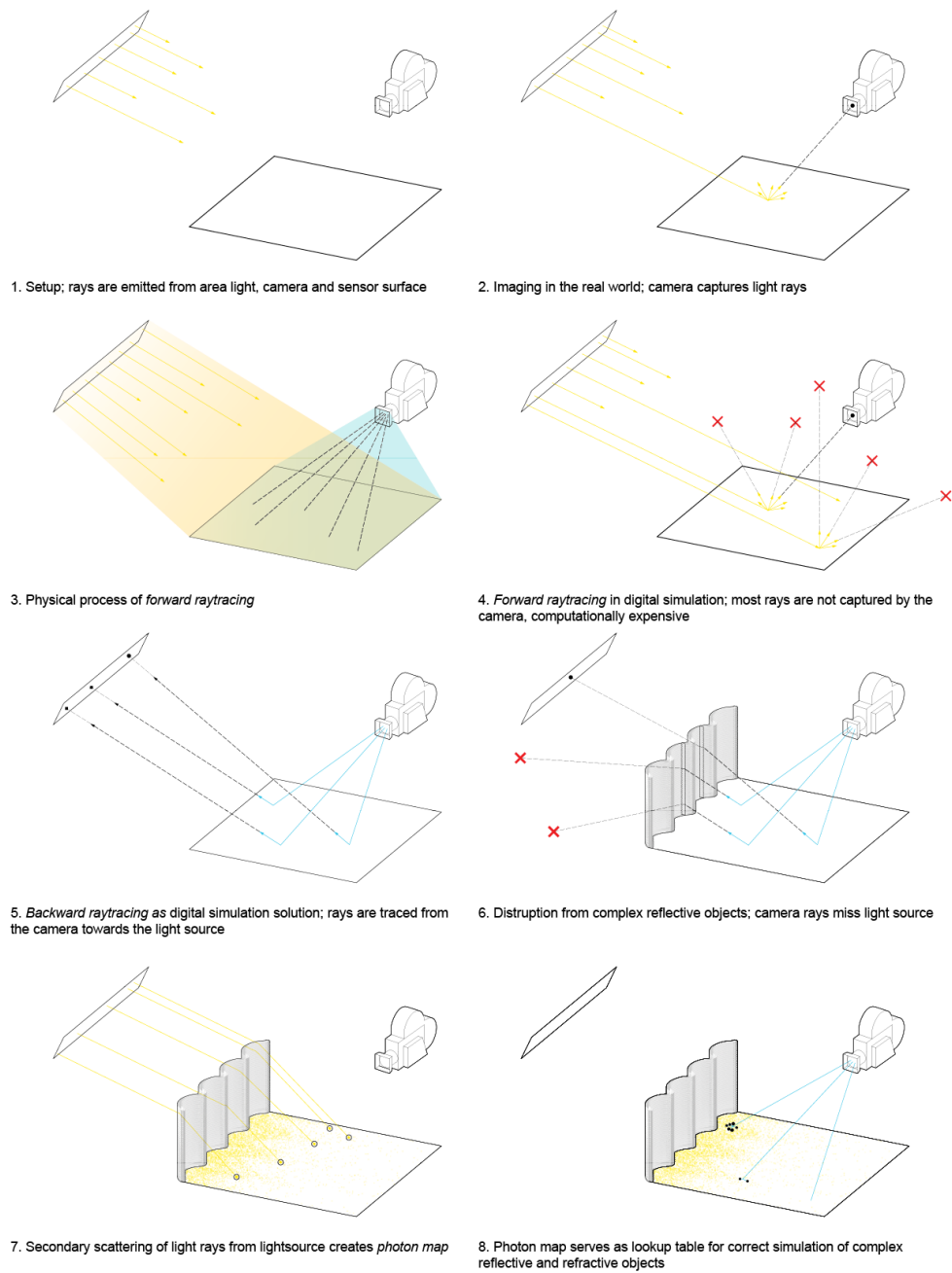


Figure 1: Light behavior in the real world 1-3, as compared with traditional digital simulation methods 4-6 and the photon mapping approach 7-8.

Research in computer graphics has shown how geometry and depth of a transparent acrylic sheet can be shaped to create custom caustic effects at a fixed distance (Kiser et al. 2012; Papas et al. 2012). The described algorithmic process is used for a purely speculative architectural proposal to create a large ornamental caustic reflection (Kiser et al. 2012). This thesis, in comparison, will take the unique constraints of real-world additive manufacturing of glass into account.

Advances in environmental simulation allow for accurate prediction of light scattering through transparent glass components. In the course of this research, a method of using high dynamic range (HDR) photographs to calibrate daylight simulations (Jones and Reinhart 2017) and the *Radiance* render engine (Ward, G. and Shakespeare 1998) have been used with a photon mapping extension (Schregle 2004) to simulate highly geometrically complex architectural components.

A new relationship between the environment and architectural matter is proposed. The design framework builds upon existing methodologies of temperature, climate, and energy (Lally 2009, 2014; Banham 1969; Martin and Graham 2016; Benjamin 2017) and extends them to use light as the main design actor. With additively manufactured optically transparent glass as the main material actor, the light and the glass structure perform beautiful new interactions.

3 Photon Mapping of Geometrically Complex Glass Structures: Methods and Experimental Evaluation¹

Ramon E. Weber^a, Christoph Reinhart^b, and Neri Oxman^a

^a Mediated Matter Group, MIT Media Lab, Department of Architecture and Urban Planning

^b Sustainable Design Lab, Department of Architecture and Urban Planning

3.1 Abstract

Advances in digital fabrication and additive manufacturing have enabled the creation of geometrically complex glass structures and building components, opening up new design opportunities across scales. Quantifying and evaluating their optical performance, however, remains a technical challenge. In order to accurately predict light behavior, common approaches of daylight modelling utilizing light-backward raytracers are insufficient. This paper evaluates the use of the photon mapping approach within the *Radiance* render engine to simulate artificial and natural lighting conditions. 3D printed optically transparent glass components are used to benchmark the simulations. We present a workflow to gather geometric data of the glass objects and a series of validation experiments. Pairs of physical studies and digital simulations are compared to assess optical performance in the context of both indoor and outdoor lighting conditions. These experiments demonstrate that the photon mapping approach can reliably measure and predict caustic light patterns and indoor light levels with some limitations, specifically of glare and scattered light from the glass objects themselves.

3.2 Introduction

Lighting the built environment is one of the foundations of modern life with direct consequences for our everyday experiences, the environment, and workplace productivity. The way we choose to light the interior of our buildings, using a combination of daylight and electric lighting, quite literally determines how and what we see. However, electric lighting

¹ A version of this chapter is currently under review as:

Weber, Ramon E., Christoph Reinhart and Neri Oxman. 2020. "Photon Mapping of Geometrically Complex Glass Structures: Methods and Experimental Evaluation" In *Building and Environment*.

comes at a significant cost, accounting for 17% of U.S. energy use in commercial buildings (Woodward 2017). Daylighting has been widely promoted, not merely as an electric lighting replacement, but as a superior source of lighting due to its spectral qualities, ability to offer views, and temporal variability that links building occupants to the outside. While increasingly dense urban environments challenge access to daylight for all, thoughtful urban zoning and building massing approaches can support good daylight penetration even in unusually dense urban environments (Saratsis, Dogan, and Reinhart 2017). In order to explore lighting and daylighting concepts in non-standard situations, architectural design teams routinely rely on an ever-expanding suite of simulation tools for both electric lighting as well as daylighting design (Ochoa, Aries, and Hensen 2012). While a variety of simulation approaches exist for modeling daylight, the open source light-backward raytracer, *Radiance* (Ward, G. and Shakespeare 1998), written by Greg Ward at Lawrence Berkley National Laboratory, has dominated the field of sustainable building design for decades (Galasiu and Reinhart 2007). Part of the appeal of *Radiance* is that it has been extensively validated vis-à-vis measurements in full-scale mockups both for illuminance distributions (Mardaljevic 1995; C. F. Reinhart and Walkenhorst 2001; C. F. Reinhart and Andersen 2006; McNeil and Lee 2012) and high dynamic range (HDR) luminance distributions (Jones and Reinhart 2017). Furthermore, non-expert user-friendly implementations of *Radiance* in popular software tools such as DIVA (J. Alstan Jakubiec and Reinhart 2011) and Ladybug Tools (Sadeghipour and Pak 2013) are becoming popular amongst architects and engineers and enable predictions of daylight availability or glare during the building design process.

However, as with any light-backward raytracer, *Radiance* cannot reliably model light-concentrating phenomena such as caustics from lenses or curved highly specular surfaces. To model caustics, a photon map extension was implemented into the *Radiance* environment by Roland Schregle (Schregle 2003, 2004). Photon mapping consists of two steps where light photons are initially emitted from a light source into a scene and then collected (gathered) in a secondary regular backward raytracing step.

The aim of our research is to evaluate the ability of the photon mapping approach to accurately predict light distributions caused by curved glass objects. Our validation consists of a series of comparative physical measurements and digital lighting simulations. Using 3D printed glass geometry as the benchmark for light-redirecting building components, our tests evaluate real-world physical artefacts of high geometric complexity. In order to accurately benchmark the digital simulations, digital-physical pairs of the experimental setups were used.

Current trends in architectural design require novel digital design tools that enable the engineering and fabrication of geometrically varied building components in high profile

buildings. Curved building envelopes such as the King Abdullah Financial District Metro Station in Riyadh, designed by Zaha Hadid Architects (ZHA) with complex glazing systems and reflective metal façade elements, challenge existing lighting simulation frameworks (Figure 2). In order to fully leverage the new geometric freedom to construct spaces with superior environmental performance and occupant well-being, lighting simulation capabilities must also expand.



Figure 2: Geometrical complexity in a glazed building envelope, King Abdullah Financial District Metro Station in Riyadh, designed by Zaha Hadid Architects. Exterior rendering (left), construction of façade diagrid (middle, photograph by Faisal Bin Zarah) and close-up of detailed facade mockup (right) (all images property of RDA and courtesy of ZHA).

Previously tested approaches for modeling and simulating light behavior in so-called complex fenestration systems (CFS) include the use of Bidirectional Scattering Distribution Functions (BSDF) that have been successfully modeled and implemented into the *Radiance* platform to accurately depict reflective window blinds (Konis and Lee 2015), optical louver systems (McNeil and Lee 2012), prismatic window film (McNeil, Lee, and Jonsson 2017) or the use of function files for laser cut panels (LCP) (Greenup, Edmonds, and Compagnon 2000; Grobe 2019). A BSDF is a four-dimensional mathematical function that describes the optical transmittance or reflectance of a material for all combinations of incoming and outgoing rays. BSDFs are determined via modeling or measurements in a goniophotometer (Andersen and deBoer 2006). As a further challenge, even if a goniophotometer is available, for some samples with pronounced specular or caustic components, it remains difficult to detect peaks within the distribution. In addition, goniophotometers accommodate limited sample sizes, assuming that the optical behavior of larger components is the same as that of the sample. *Radiance* function files allow users to define specific mathematical functions that describe the light-redirecting behavior of a material (“The RADIANCE 5.1 Synthetic Imaging System” n.d.). Furthermore, combining BSDF based lighting simulations with EnergyPlus models allows for the development of both daylight redirecting and energy harvesting systems (Vlachokostas and Madamopoulos 2017).

For more complex building envelopes, where material parameters and geometry vary across a surface, BSDF and function file methods cannot be reliably applied. In order to represent and simulate the performance of parametric façades with highly differentiated geometries, photon mapping offers an alternative approach by considering the complete digital geometric representation of a system of any size.

Ongoing advances in additive manufacturing have led to the development of novel material systems that could be further developed for use as architectural components towards large-scale applications in the built environment. Out of their research around additive manufacturing of optically transparent glass, the Mediated Matter Group at the MIT Media Lab created a manufacturing platform for the fabrication of large-scale components (Figure 3).



Figure 3: Additive manufacturing of optically transparent glass by the Mediated Matter Group, MIT Media Lab. Glass object with caustic pattern (top left), 3D printing process (top right), variety of printable objects (bottom left) and glass column with inserted light (bottom right) (all images courtesy of the Mediated Matter Group).

Such an extrusion-based 3D printing technology enables the use of computer-aided design (CAD) models (Klein et al. 2015) to specify geometry and surface structure of glass components. Unlike the flat float glass that is traditionally used in buildings, 3D printed glass has an inherent depth and surface geometry that can be customized across every element. The optical clarity of glass creates highly complex caustic patterns when light is projected through a printed object. Curvature and surface texture, which consists of striations and bulges caused by the 3D printing process, offer a high degree of control over the reflection, redirection, and shading of light passing through the transparent objects (Inamura et al. 2018). It should be

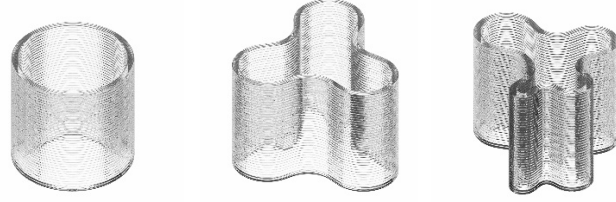
noted that even though the manufacturing process is digitally controlled, 3D printing of glass currently creates unforeseeable extrusion details on the millimeter scale that add to the aesthetic appeal and uniqueness of each sample but cannot be fully predicted in advance. In order to create reliable digital pairs of the test objects that were investigated in this study, the authors used post-processed 3D scans of the printed objects that emulated these extrusion details (see below).

When deployed in a real-world context, possible visual discomfort, glare, as well as light and shadow of a transparent object must be considered in its design. For this study, the authors therefore collected HDR photographs and photon map-based simulations of 3D printed objects under a variety of electrically lit and daylight conditions. In HDR images, each pixel has an RGB color value as well as an absolute luminance value. The authors then used the images to evaluate whether photon mapping can be used for simulating both a 3D printed object's overall architectural appearance as well as its impact on visual quality and comfort in the surrounding space.

3.3 Methodology

3.3.1 Validation Experiments

For the benchmarking exercise described above, three 3D printed glass objects were used: a standard cylindrical tube, a symmetrical three-bulge extrusion, and an irregular four-bulge extrusion (Table 1). As a result of the additive manufacturing process, the objects feature a rippled layering on their exterior surface with visible layers at 5 mm intervals. The interior of the objects consists of solid glass without defects or layering, enabling full optical transparency. The geometric complexity of the rippled layering, in combination with the freedom of form enabled through the manufacturing process, creates glass pieces with highly complex doubly curved lens geometries. This makes the prediction and simulation of light behavior passing through a component computationally expensive and inherently difficult.



Object Nr.	1	2	3
Description	Cylindrical Tube	Three Bulges	Four Bulges
Dimensions	217 x 217 x 209 mm	262 x 283 x 201 mm	231 x 245 x 201 mm
Polygon mesh face count	263783	244668	237827

Table 1: Comparison of 3D printed glass objects used in validation experiments.

The authors conducted two sets of experiments to validate the photon map:

- Experiment A: Digital-physical pair of glass objects under a single light electric light source
- Experiment B: Digital-physical pair of glass objects under variable daylight conditions

To capture the lit scenes and the physical quantity of luminance, as per the protocol presented by Inanici and Galvin, and Jones and Reinhart (Inanici and Galvin 2004; Jones and Reinhart 2017), a series of photographs were combined into an HDR image where the pixel brightness per image was matched with the measurements taken from a luminance meter. To record our physical experiments, a Canon EOS 5D Mark III full-frame digital camera outfitted with a 24-70 mm F2.8 Canon lens and a Konica Minolta LS-110 luminance meter were used.

3.3.2 *Experimental Setup A: Interior Lighting*

The first experimental setup consisted of a series of 3D printed glass objects (Table 1: Object Nr. 1, 2, 3) that were centred on an 80 x 80 cm grid for reference purposes (Figure 4). The digital camera is mounted vertically on an aluminium scaffold above the test objects to capture the caustic patterns with as little distortion as possible on the flat grid. A luminance meter is used to calibrate each photograph. Additionally, a reference image without a glass piece was taken to show the distribution of light without caustic reflections. In blacked out surroundings, a single light source was directed towards the glass pieces: A Soraa PAR 20 10.8 W spotlight was placed 22 cm above the ground plane, over the centre of the grid.

3.3.3 *Experimental Setup B: Exterior Lighting*

The daylighting conditions were tested in Cambridge, Massachusetts, USA on the roof of the MIT Media Lab (42°21'36.9"N, 71°05'14.9"W). To mimic an architectural interior space with a 3D printed glass envelope, an enclosure of 72 x 102 x 21 cm was constructed with an opening that fit the cylindrical glass tube (Table 1: Object Nr. 1). The glass tube was placed on the side of the space and blocked the only direct light into the space (Figure 5). On the back side of the box, a Canon EOS 5D Mark III full-frame camera with a 24-70mm F2.8 Canon lens was mounted on a tripod and placed at the secondary opening to record images of sunlight passing through the glass cylinder. Data was captured through HDR photographs every half hour from 08:00 to 16:00 on October 19, 2019. The sky was clear without cloud cover obstructing the sun. Continuous measurement of the luminance levels on a fixed point inside the box was conducted with the Konica Minolta LS-110 luminance meter.

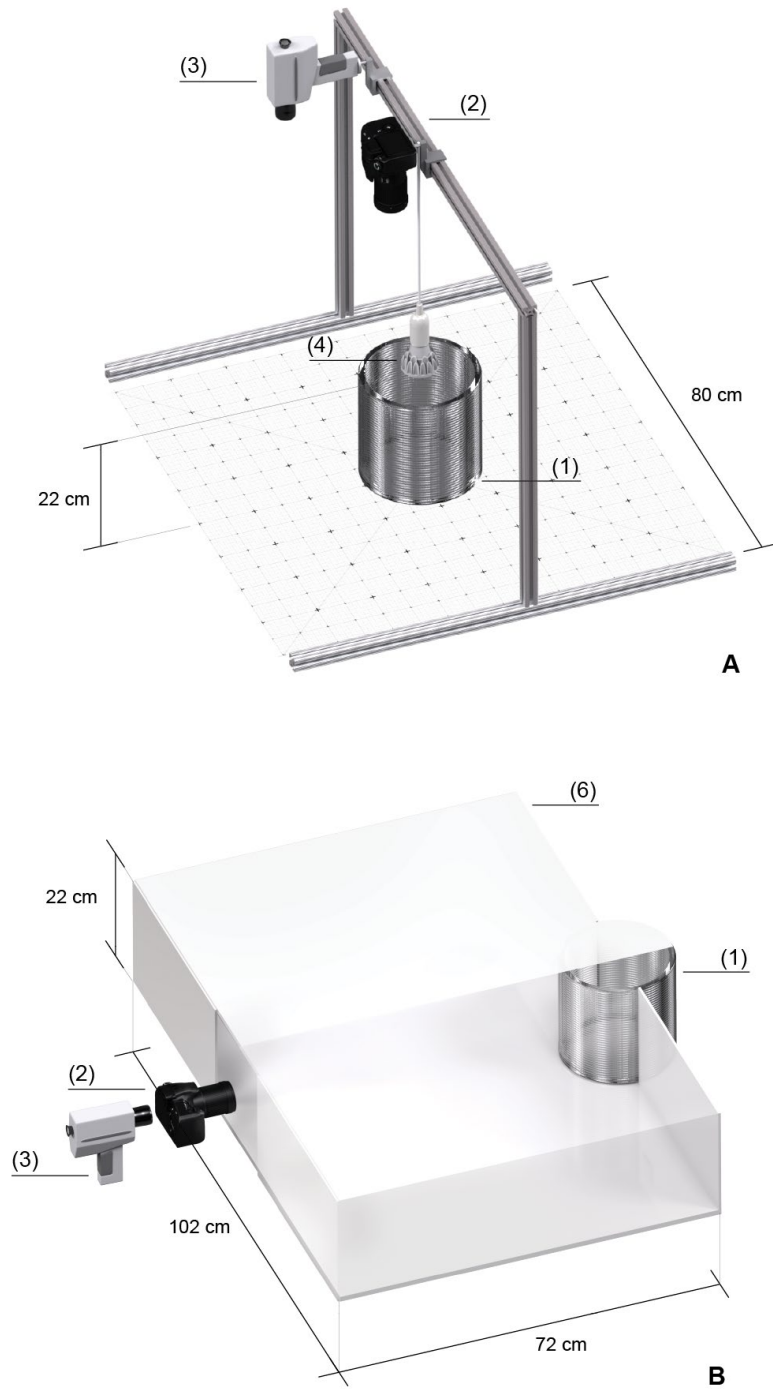


Figure 4: Schematics of experimental setups A and B with 3D printed glass object (1), digital camera (2) and luminance meter (3). Experiment A is set up in an indoor environment with the artificial light source, Sora Par20 10.8W (4). Experiment B is conducted in a closed box (6) in an outdoor environment.

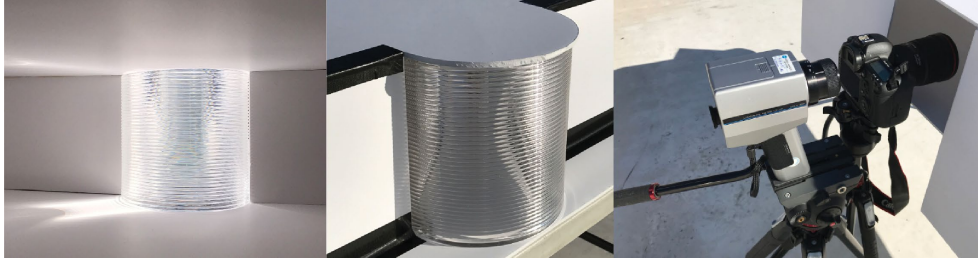


Figure 5: Photographs of physical setup of experiment B with interior view of lit cylinder (left). An exterior view of the 3D printed glass cylinder in sunlight (middle) and the measurement via digital camera, Canon EOS 5d Mark III and the Konica Minolta LS-110 luminance meter (right).

3.3.4 Geometry Workflow

Although deposition of the glass in the manufacturing process has proven to be highly precise (Klein et al. 2015), the actual geometry of a 3D printed glass object exhibits artefacts that stem from temperature and viscosity fluctuation in the manufacturing process. To create a high-resolution mesh that accurately represents the surface detail of a 3D printed glass piece, a digital post-process had to be developed, as shown in Figure 5. The workflow illustrates how a fine geometric detail was applied to a simulation geometry of a larger scale. In this case, a 3D printed glass sample part with a layer height of 5 mm in combination with an abstract input geometry was used to create a digital model of each physical object shown in Table 1.

Because of the dimensions of the 3D glass prints used in our physical experiments, a full 3D scan proved to be technically unfeasible with available equipment. Scanners or photogrammetry methods that are used for large scale objects fail to capture the detail of the 3D printed layers that are needed for an accurate digital simulation. A state of the art Artec Leo 3D scanner (Artec3d 2020) was tested and did not provide the required surface details. As a result, we construct our workflow around 3D scanning of a sample piece, small enough to be able to be scanned with a laser scanner on a rotary bed. The sample piece with the dimensions 16 x 73 x 49 mm was a section cut from a larger 3D printed cylinder and the same print parameters as our test pieces, ensuring the same layer heights and thickness. As a first step (a), a NextEngine 2020i 3D laser scanner is used to capture the detail of a small 3D printed glass sample. For the laser to detect the surface of the sample, the glass is coated using a water soluble SKD-S2 Aerosol Developer Spray. The surface scan data is reconstructed as a mesh using ScanStudio HD (NextEngine 2020). The triangulated mesh we retrieve has inherent noise and artefacts, such as overlapping and non-manifold mesh faces, that make it impossible to be used directly for an accurate simulation. A postprocessing step of converting the triangulated mesh into a smooth and continuous surface is needed. We conduct this re-meshing (b) using the 3D modeling package Autodesk Maya (Autodesk

2020), where the triangulated surface serves as a constraint for the generation of a quadrilateral mesh surface that approximates the noisy 3D scanned mesh of the sample part. For continuous regular layering as in our sample part the quadrilateral mesh surface can be converted into a cross section curve to smoothly represent both sides of the object as non-uniform rational basis spline (NURBS). A new input geometry is created in Rhinoceros 3D (Rhino, (McNeel & Associates 2020)) that represents the overall dimensions of the final geometry without any details (c). The input geometry has the exact dimensions of the glass test pieces (Table 1). Using a regular quadrilateral mesh or NURBS curve representation of the surface geometry of the sample part, the geometric detail of our scan can be transferred and mapped onto the input geometry with standard modeling operations (d). This results in a high-resolution mesh, creating an accurate digital model that applies the geometric detail of the sample part to our input geometry.

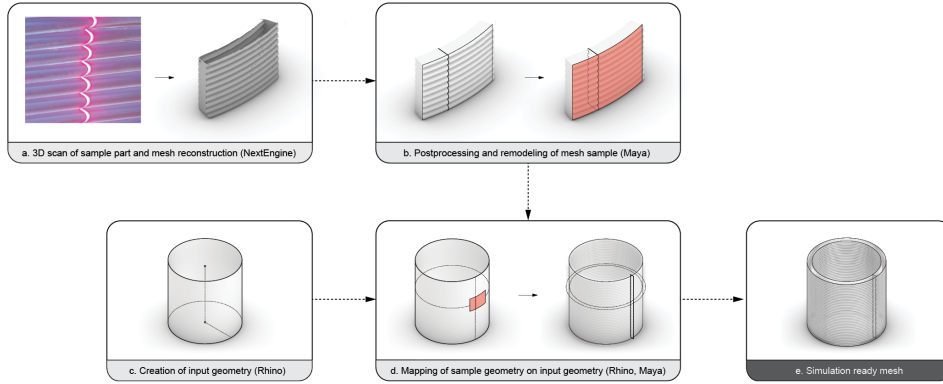


Figure 6: Remodeling workflow for 3D printed glass. A sample geometry is scanned and mapped onto a final geometry to create the mesh used in the lighting simulations (A-E).

3.3.5 Digital Simulation

A digital scene of each physical setup as described in Figure 3 was created in Rhino and exported as an OBJ file. For an accurate representation of the 3D printed glass geometry, a high-resolution mesh was produced of each glass piece using the described geometry workflow. The light simulations were produced with *Radiance* in photon mapping mode. The geometries and lights (sky and spotlight) were converted into the *Radiance* file format and assembled as a *Radiance* scene. For Experiment A, the spotlight used in the physical setup was represented using an IES file provided by the manufacturer. To test its accuracy, a calibration image using the light without any geometry was produced.

For Experiment B, the *Radiance* program *gendaylit* was used to create a sky according to the Perez sky model (Perez, Seals, and Michalsky 1993). With measurement data provided by

the MIT Weather Station, total horizontal solar radiation was first split into direct normal irradiance and diffuse-horizontal irradiance using the *gen_reindl* program in Daysim (Reindl, Beckman, and Duffie 1990) and then input into *gendaylit*. Measured radiation on October 19, 2019, a sunny day with no cloud cover, ranged from 147 kWh/m² (08:00) to 601 kWh/m² (12:25).

The *Radiance* photon map extension, developed by Roland Schregle (Schregle 2004), was used to compute the caustic reflections of the glass objects. In a first assessment, caustic photon maps in various resolutions were produced to determine an optimal photon count, balancing render speed with ability to depict the required caustic details. Photon maps were computed on a Linux machine with following specifications: *128 Gb ddr4* Ram, *Nvidia RTX Geforce 2080* Graphics card, *3.0 Ghz AMD Threadripper 2990wx* 32-Core Processor.

A sample *Radiance* command setup involves 4 steps (Table 2), consisting of scene assembly (Step 1), photon map assembly (Step 2) image generation (Step 3) and image filtering (Step 4). The *Radiance* materials for the 3D printed glass for both experiments and for the interior walls of the box in experiment B are specified in Table 3.

Step 1	oconv	{skyfile}.rad {meshfile}.rad > {scene}.oct
Step 2	mkpmap	-n 32 -t 30 -apg {globalpmapfile}.gpm 50k -apc {causticmapfile}.cpm 50m {scene}.oct
Step 3	rpict	-vf {viewfile}.vf -af {ambtempfile}.amb -x 3200 -y 2400 -ps 8 -pt .15 -pj .6 -dj 0 -ds .5 -dt .5 -dc .25 -dr 0 -dp 128 -st .85 -ab 4 -aa .15 -ar 512 -ad 2048 -as 512 -lr 4 -lw .05 -ap {globalpmapfile}.gpm 100 2000 -ap {causticmapfile}.cpm 100 2000 {scene}.oct > {rpictimage}.hdr
Step 4	pfilt	pfilt -r .6 -x /4 -y /4 {rpictimage}.hdr > {outputimage}.hdr

Table 2: Sample commands for the photon mapping approach (variable files indicated with {file})

Glass	White
void dielectric print_glass	void plastic reflective_white_box
0	0
0	0
5 0.9 0.9 0.9 1.5 0	5 0.92 0.92 0.92 0.0135 0.0000

Table 3: Radiance material definitions of the 3D printed glass material (Glass) and the box interior material (White)

3.4 Results

The following sections describe the results of the physical validation experiments, including the HDR photographs of the 3D printed glass objects and the luminance measurements used to calibrate the photographs.

3.4.1 Results of Experiment A: Indoor Lighting

Results of Experiment A are depicted in Figure 7 and Figure 8. In Figure 7, side-by-side comparisons of false color HDR photographs (physical) and *Radiance* photon map renderings (digital simulation) show how accurately photon mapping predicted light behavior. The comparison cases show the physical setup without no object as photograph (p0) and simulation (s0). The three 3D printed glass objects from Table 1 are represented as both photograph of physical setup (p1, p2, p3) and digital *Radiance* simulation (s1, s2, s3). The black grid on the ground plane of the photographs was used to center the objects and maintain reference points for the calibration. The renderings feature a white matte backdrop without a grid. Photon maps with 200 million caustic photons were rendered via the *Radiance* *-mkpmap* command. Both photographs and simulations have no post-production effects applied and were converted into false color for visual comparison purposes. They were remapped to a logarithmic (*log*) scale and a range of 1000 cd/m² with the *Radiance* *-fcolor* command. In all three cases, the overall lighting pattern on the grid below the glass objects look largely identical and include the same caustic hot spots.

Pairs of measured (physical) and simulated (digital) luminance levels across the center x-axis of the images for the same four cases are shown in Figure 8. In the photographs, the black gridlines of the calibration grid cause noise in the measured brightness plots. Noise in the *Radiance* from the photon map rendering results in slight distortions in the simulated brightness plots. Brightness values were obtained using the *Radiance* image analysis tool - *pcomp*. They are shown in a logarithmic scale for both measured and simulation. For more accurate comparisons, the curves were scaled and centered to adjust for slight deviations in the digital representation and to more accurately map the features of the physical tests. In order to minimize offsets from the noise from both gridlines and simulation, the data was filtered using an average smoothing and capped at a maximum of 1000 cd/m². The resulting curves were processed and have a root mean square of 16.7 % (test 0), 18.12 % (test 1), 7.97 % (test 2), 12.91 % (test 3). The resulting luminance sections exhibit largely similar behavior, except that the measured peaks tend to be somewhat more pronounced than in the simulations, whereas grain from the noise in the photon map distorts the results of the simulation slightly.

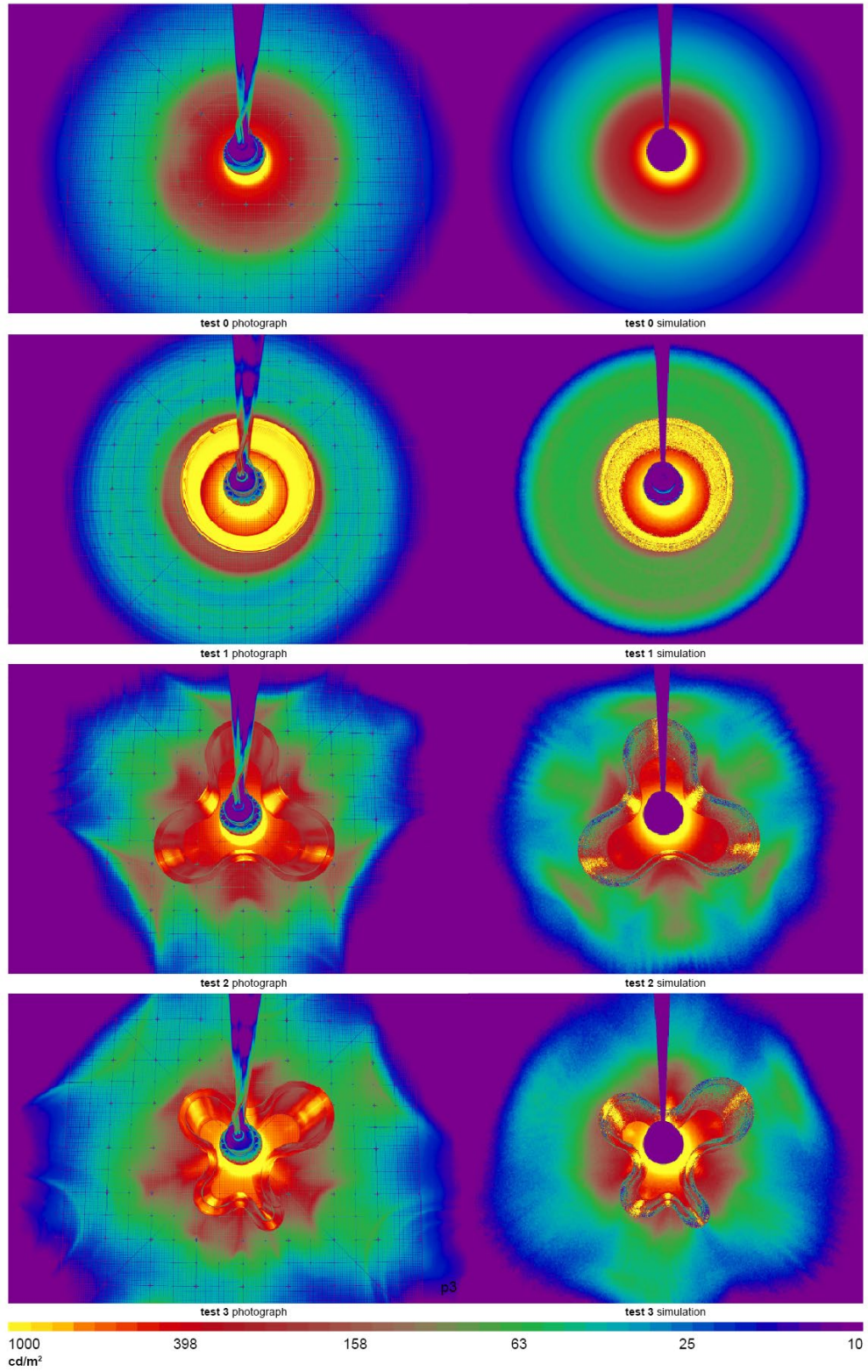


Figure 7: Comparison of HDR photograph and Radiance photon map simulation of no object (test 0), cylindrical tube (test 1), three bulges (test 2) and four bulges (test 3).

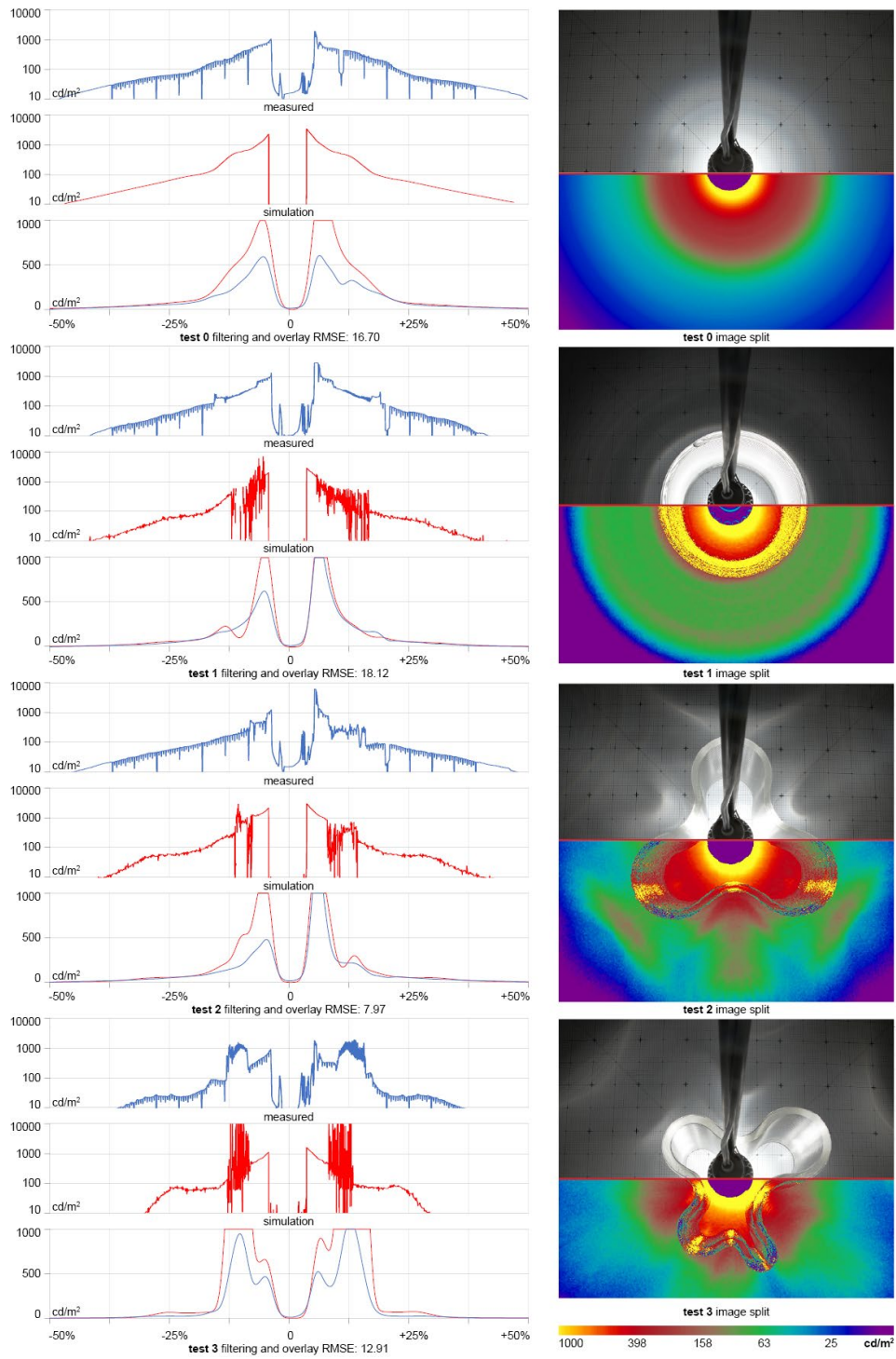


Figure 8: Plots of brightness values (left) with measured and simulated luminance in logarithmic scale and a smoothed, scaled and capped overlay of both datasets in linear scale with the resulting root mean square error. Image split (right) shows an HDR photograph overlaid on the digital simulation with a red line indicating the position of the luminance measurements in the plots.

3.4.2 Results of Experiment B: Exterior Lighting

Results of Experiment B are depicted in Figure 9. Qualitative comparisons show how the complex simulated (digital) caustic reflections exhibit the same patterns as their measured (physical) counterparts. Side-by-side comparisons of false color renderings and HDR photographs depict how higher concentrations of light at the top and bottom of the glass cylinder are always visible in both photograph and rendering. A key difference between photographs and renderings is the appearance of the glass itself as a source of glare. In the *Radiance* photon mapping simulation, the glass appears dark and only passes light into the interior. In a high resolution simulation there appears to be significant noise in the areas with glass material in the simulation where some pixels would attribute to the glare. When scaling down the image, this information is not retained.

It should be noted that additional light-reflective structures in the physical environment were not simulated digitally. Although the experiment was fully exposed to sunlight and not shaded at any part of the day, additional secondary bounces of light through the camera hole and through the glass from additional surrounding objects were not considered. Furthermore, the simulation only considered a fixed set of ambient bounces that lit the space, so lighting levels may differ.

Figure 10 shows a comparative graph of luminance measurements of the *Radiance* simulation. The physical measurements with the luminance meter differed up to $\pm 15\%$ each time they were taken. Averages of three measurements taken at the same point at the same time are shown as data points of the measurements. To match the digital and physical measurements as closely as possible, an aerial average of a patch of approximately 25 cm^2 around the physical measurement point was averaged to obtain the digital simulation light luminance value from the calibrated *Radiance* image. The graph shows that the light levels in the interior of the box were predicted highly accurate. Furthermore, visual glare with a threshold of $> 2000 \text{ Cd/m}^2$ was predicted successfully for all times of the day.

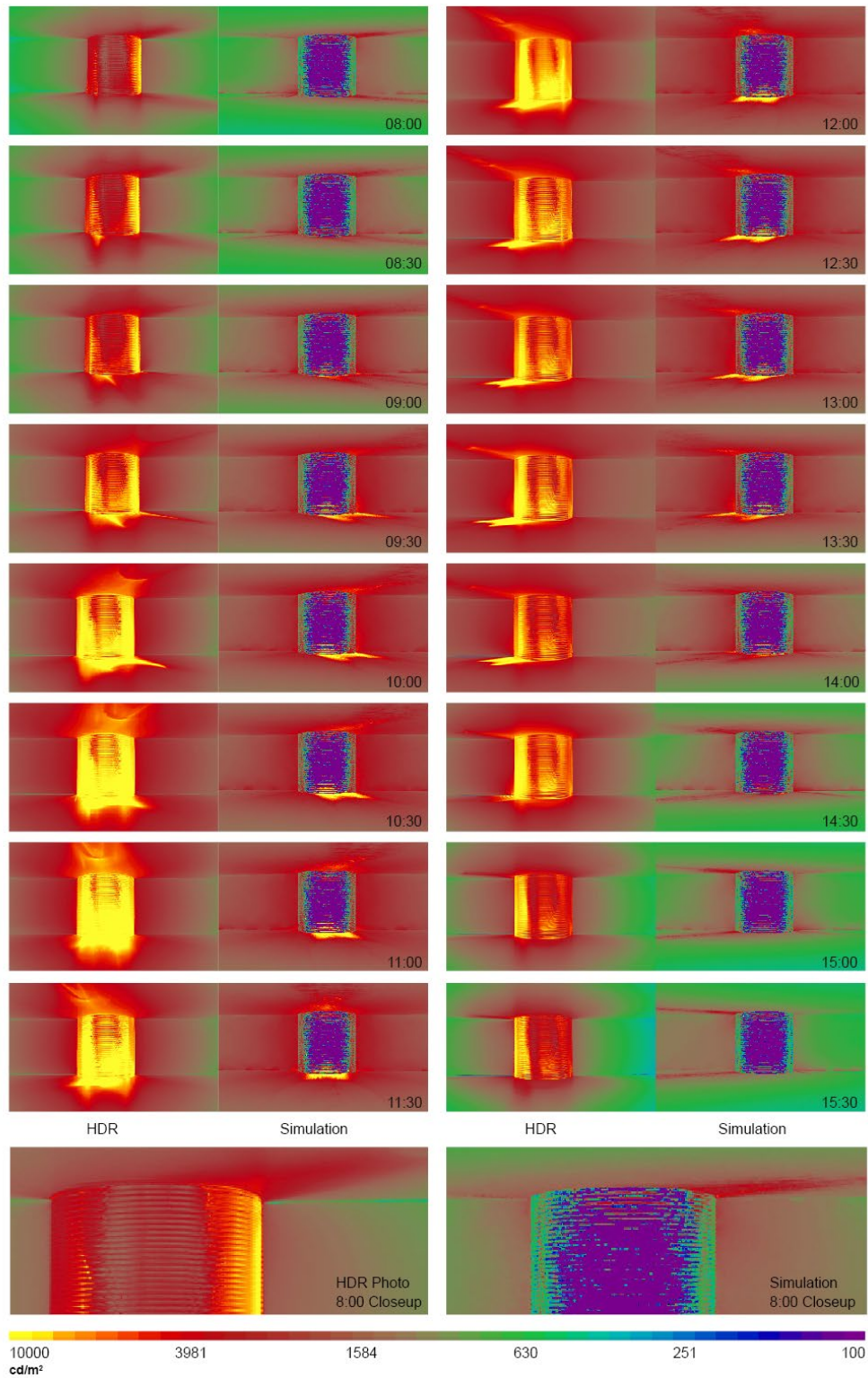


Figure 9: 3D printed glass cylindrical tube in daylight captured as false color HDR photographs and *Radiance* photon mapping simulations.

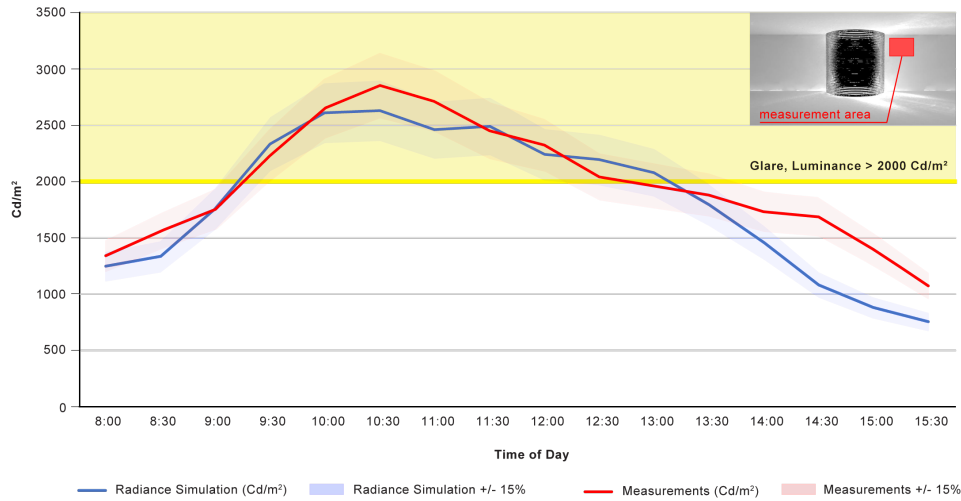


Figure 10: Light level comparison, Cd/m², of a fixed point inside the box in Experiment B of both digital Radiance simulation and physical measurements. A sample image of the digital Radiance simulation at 9:30 am is depicted (top right corner). The red square indicates the area of where the luminance value average was measured. A visual glare threshold of > 2000 Cd/m² is displayed in yellow.

3.5 Discussion

The results indicated that the photon mapping approach is able to reliably simulate certain aspects of light distributions through complex 3D printed glass objects. Most notably, the method excels at predicting lighting patterns resulting from such objects as artistic luminaires or daylighting façade elements. It unfortunately is subject to the same limitation of other raytracing methods in that they generally fail to model scattering at the glass surface or within the glass due to material imperfections. Such scattering phenomena may lead to extremely high luminances, which are equally prone to trigger delight and glare. The authors attempted unsuccessfully to model the light scattering in *Radiance* by testing a series of material modifiers with varying roughness and indexes of refraction. Similar limitations were previously reported by Greenup, Edmonds, and Compagnon when they tried to simulate scattered lighting artefacts from laser cut panels (Greenup, Edmonds, and Compagnon 2000). Real-world fine-grained material imperfections inside materials can have large effects on light scattering and thus glare, making the latter extremely difficult to simulate.

In our Experiment B, light distribution in the daylit space itself created so much glare along the surrounding walls that traditional glare modeling methods predicted visual discomfort would occur at the same time for measurements and simulations (Figure 10). However, because the daylighting element itself was not detected as a glare source, one can easily imagine situations – e.g. in the presence of dark walls – in which the room does not contribute

to glare. In this case, glare and visual discomfort would remain undetected by the photon map.

What do these results mean for designers? The authors recommend using the *Radiance* photon mapping approach for aesthetic explorations. Visual comfort studies should further pair digital models with physical explorations of parts of a façade or building. The following sections present additional modeling advice for setting up lighting simulations for complex 3D printed glass objects.

3.5.1 Geometric Detail

Successful simulation of complex geometries using *Radiance* photon mapping requires a highly accurate digital model. Capturing or modeling all relevant detail can require a significant effort. In the case of additive manufacturing, an abstracted design model is therefore not sufficient for simulation, even when it might be used in manufacturing of the object. Rather, the model must represent the physical outcome of the manufacturing process, including all significant geometric details. As shown in the presented research, a process like 3D printing glass must consider significant uncertainty due to material layering and composition. The 3D scanning and remodeling workflow in Figure 6 lends itself to the digital representation of such highly complex geometries. The geometric freedom enabled by additive manufacturing further increases the strain on a simulation engine. 3D scanning and accurate modeling are key steps in accurate high-resolution representation of complex geometries and their successful simulation.

Since the *Radiance* render engine relies on mesh geometries, it is important to consider the conversion process when working with NURBS geometry (for example by utilizing the Diva components inside of Rhino). An automatic conversion (e.g. by using an uncontrolled meshing operation) can lead to highly inaccurate results as shown in Figure 11, where two mesh geometries are compared. Automatic triangulation of a low-resolution mesh (a) did not suffice to accurately depict the caustic reflections. A manual adjustment and lowering of the maximum edge lengths in the meshing process created a mesh with higher resolution, successfully predicting continuous caustic patterns.

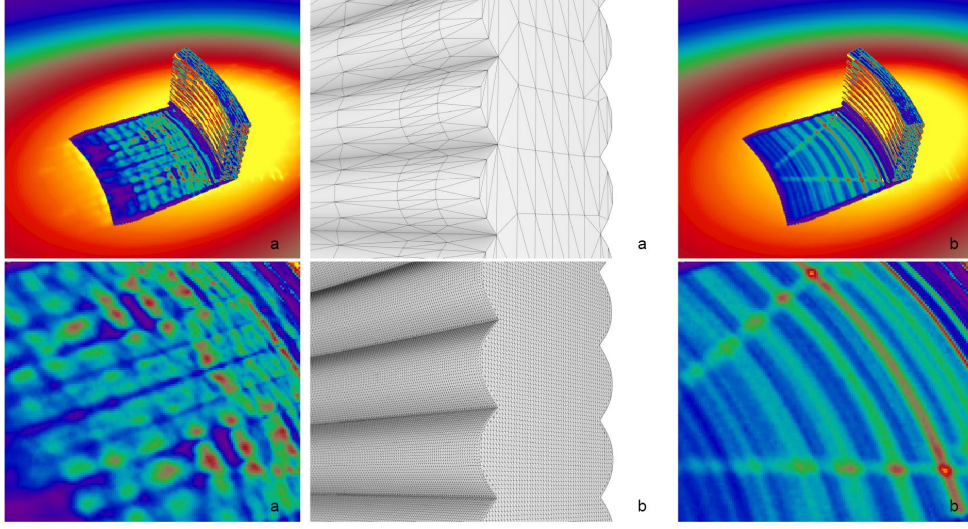


Figure 11: Sources of error through low resolution mesh representation for the number of photons scattered in the scene. A low-resolution mesh (a) with 4915 faces is compared with a high-resolution mesh (b) with 370252 faces.

3.5.2 Simulation Parameter Settings

As in the case of classic light-backward raytracing with *Radiance*, simulation parameters need to be set in accordance with the complexity of the problem at hand. For photon mapping, an adequate photon count must be chosen to be able to fully depict caustic details. For novel geometric structures, photon count must be determined iteratively and is difficult to predict, as a rule of thumb. It is dependent on the level of detail of the geometry and the lighting situation. For example, a comparative rendering in Figure 12 shows how photon count visibly increases in direct relation to the accuracy and resolution of the caustic map. We experienced a variety of simulation times depending on the photon count and the mesh resolution, ranging from five minutes to two hours. In the generation of the photon maps we made use of the multiprocessor capabilities implemented in the “-mkpmap -n” function, which makes it possible to run the photon mapping on 32 cores simultaneously.

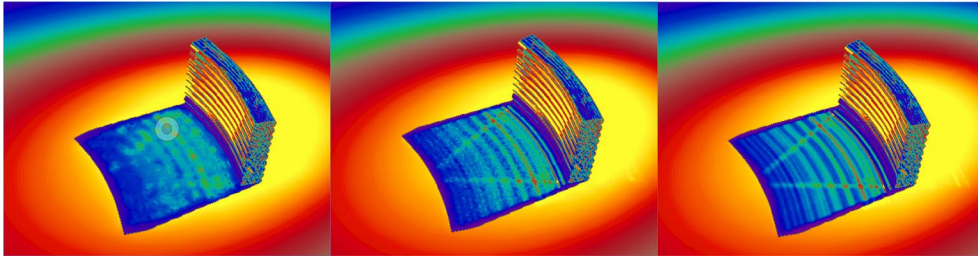


Figure 12: Photon maps (left to right) with 10000 photons, 200000 photons and 10000000 photons increase the resolution and accuracy of the caustic simulation.

3.5.3 Opportunities for Design

Reverse modeling of caustic lighting effects could enable future architectural components that can be shaped by real-world lighting properties while accounting for material imperfections. Our 3D scanning and modeling workflow can scale to fit a wide range of geometric features or geometrically complex building components and to various transparent materials. It enables daylight-conscious design and performative validation of novel architectural façade solutions or solar reflectors. It creates new opportunities for modeling irregular Fresnel lenses and curved mirror systems for light redirection and energy generation, including artistic exploration of glass technologies at the building and urban scales. Creating accurate virtual models of caustic reflections is a fundamental step in the production of 3D printed glass and other physical artefacts.

3.6 Conclusion

Daylight is a key factor in designing low-energy buildings and façades conscious of the environment and its inhabitants. Digital fabrication and additive manufacturing increase the parametric variability and adjustability of building components without further cost, and the full potential of these technologies cannot be realized without digital workflows that are able to leverage this geometric freedom into more performative building solutions.

Our research suggests that the *Radiance* toolset with the photon mapping approach to simulation provides the designer a clear idea of caustic patterns and light levels of interior spaces in highly complex glass systems. While we were able to predict when glare would occur within the space with some level of confidence, it should be noted that our simulations systematically underestimated brightness levels from the glass objects. One possible explanation is that raytracing generally, and photon mapping specifically, are not able to model light scattering due to material imperfections both at the surface and the interior of glass structures. Such material imperfections may result in objects where the glass structure itself can act as the glare source. By using digital and physical models complementary, ideally on a 1:1 scale, designers can study these effects in isolation before implementing their innovative lighting and daylighting systems in an entire building.

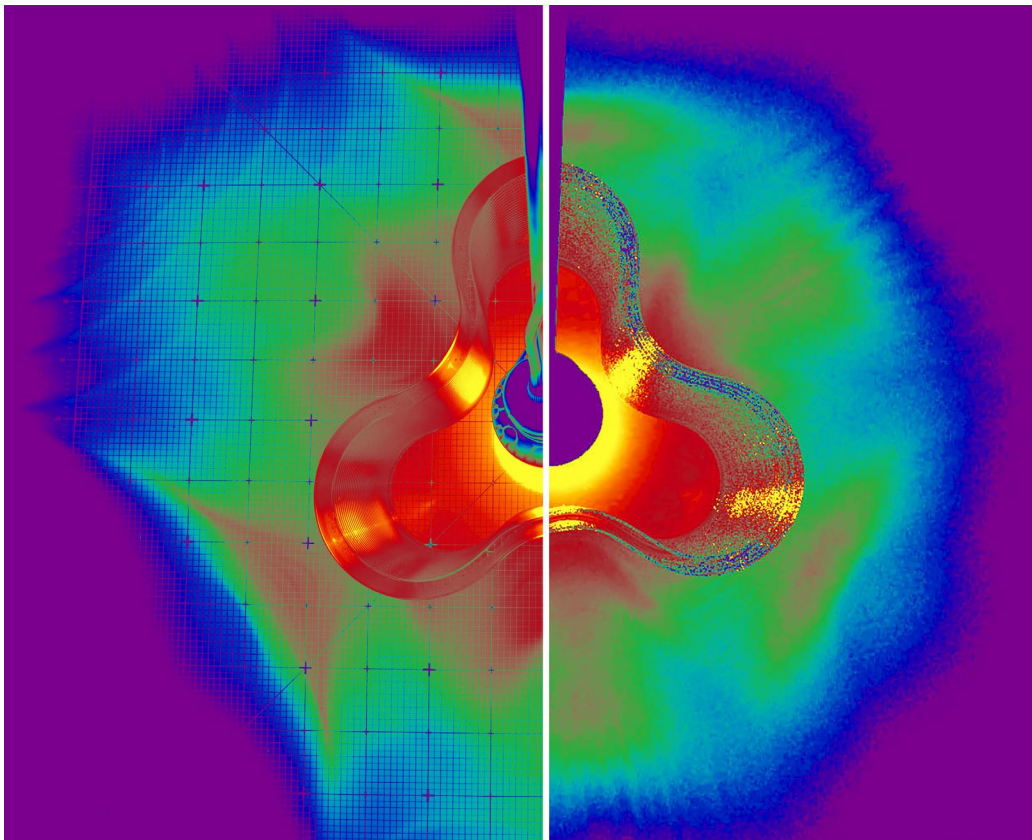


Figure 13: Comparison in falsecolor scale of HDR photograph (left) and Radiance photon map simulation (right).

4 Programmable Caustics

Utilizing machine learning and design space exploration for the design of caustic patterns in additively manufactured glass

4.1 Introduction

This chapter aims to leverage machine learning for the creation of caustic patterns of 3D printed glass objects, exploring the relationship between geometry and light. Precedent research by the Mediated Matter Group (Klein et al. 2015) has shown how optically transparent glass objects can be 3D printed using an extrusion-based method. 3D printed glass has a unique layered structure with variations in thickness and geometry. These geometric parameters influence the refraction of light and generate highly ornamental caustic patterns.

While a range of research has been conducted on exactly how to reverse engineer caustic effects to project custom images onto smooth surfaces (Kiser et al. 2012) and on goal-based caustics with micro patches (Papas et al. 2011), this thesis will take the unique constraints of additive manufacturing of glass into account. The present research focuses on creating fast predictions, visualizations, and novel ways of exploring multidimensional design spaces with machine learning.

4.2 Methods

4.2.1 *Modeling of Simplified Design Space*

First, a minimal ray tracer was implemented in Python and Grasshopper, a node-based scripting environment for Rhino to test the relationship between light and geometry. For this, a series of simple lenses (abstracted as a sphere) with variable diameter and depth, were aligned on one axis, in a fixed distance to an image plane that captured the light rays diverted by the lens. The design space embodied the geometric relationship between the sphere and the output image. Corresponding ray scatter maps with their lenses were further mapped in a design space visualization to show a variety of producible shapes. A target was introduced to direct the light to a centroid on the image plane in order to simplify the parameters. The small number of collected datapoints, can be interpolated into a larger dataset, creating a so-called surrogate model. The sample raytraced image of the configurations was then compared to a reference image and the difference was output as the sum of the quadratic mean between the two images. Various mappings of the design space using grid, threshold, and Latin-Hypercube projected the variation into the unit cube.

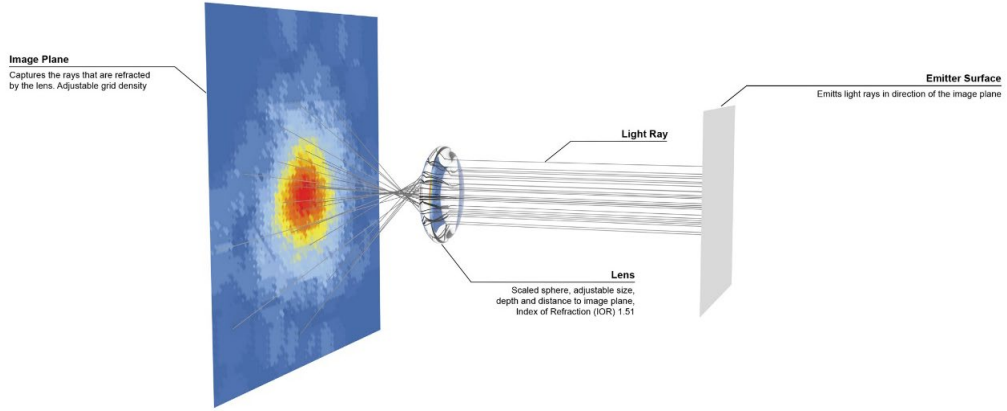


Figure 14: Setup of minimal raytracer to evaluate lenses where light rays are projected from an emitter surface through the lens and captured by an image plane.

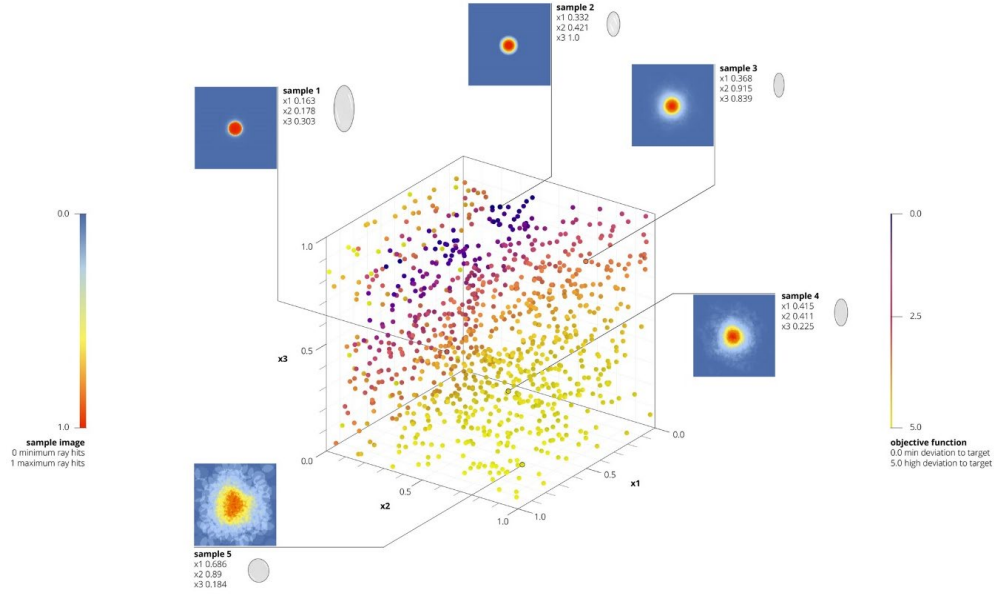


Figure 15. Design space exploration of lens geometry and their corresponding caustic pattern

4.2.2 Geometry Constraints of Additively Manufactured Glass

Increasing the complexity of the refracting lens, its geometry was linked to the geometric constraints of the existing additive manufacturing fabrication technology of glass. The 3D printing process requires a continuous toolpath from start to finish, which is achieved by a spiral toolpath along the Z-axis. This, in turn, requires closed lofted geometries as an input for the g-code generation. Each physical motor of the 3D printer has a limited turning radius, which defines the maximum curvature of the base curves. Further constraints were not considered to let the complexity and variety of the design space increase significantly. Glass,

as a highly viscous material with specific thermal properties, cools substantially after it is deposited by the nozzle. For each new layer to sufficiently melt into the previous one, the previous layer must have a specific temperature when the nozzle deposits new material on top. This requires the toolpath for a full turn to have a certain minimum length to allow the material to cool to the right temperature. Secondary adjustable parameters in the printing process include layer height and thickness, which can be adjusted by changing the speed and increasing the flow of the material, all resulting in unique textures, visual appearance, and caustic reflection patterns of the objects.

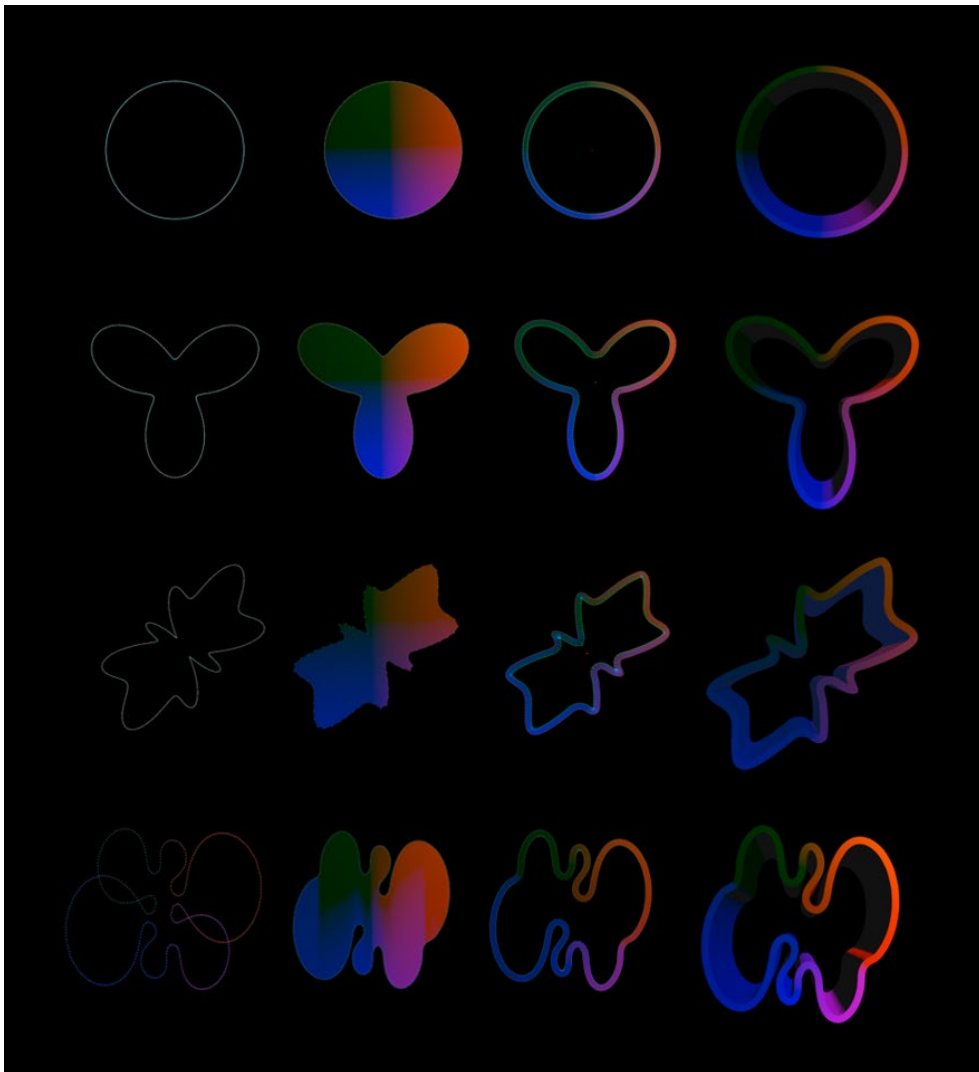


Figure 16. Parametric fabrication-aware boundary creation and extrusion workflow for the source glass geometries

4.2.3 Parametrization of Printable Geometry

A parametric model for the procedural generation of printable objects was produced. A linear combination of two Fourier basis functions with various periods and amplitudes served as the basis generator of the ground curve of the geometry. A secondary offset derived from the curvature of the curvature-weighted normal further allowed for the creation of more extreme concave and convex basic geometries. A series of geometric operations ensured that overlapping curves were resolved with a convex hull to generate closed, smooth curves along a boundary. Custom Python scripts were used to implement this behavior in Houdini (SideFX 2020) and to parametrically generate 68,355 unique geometries.

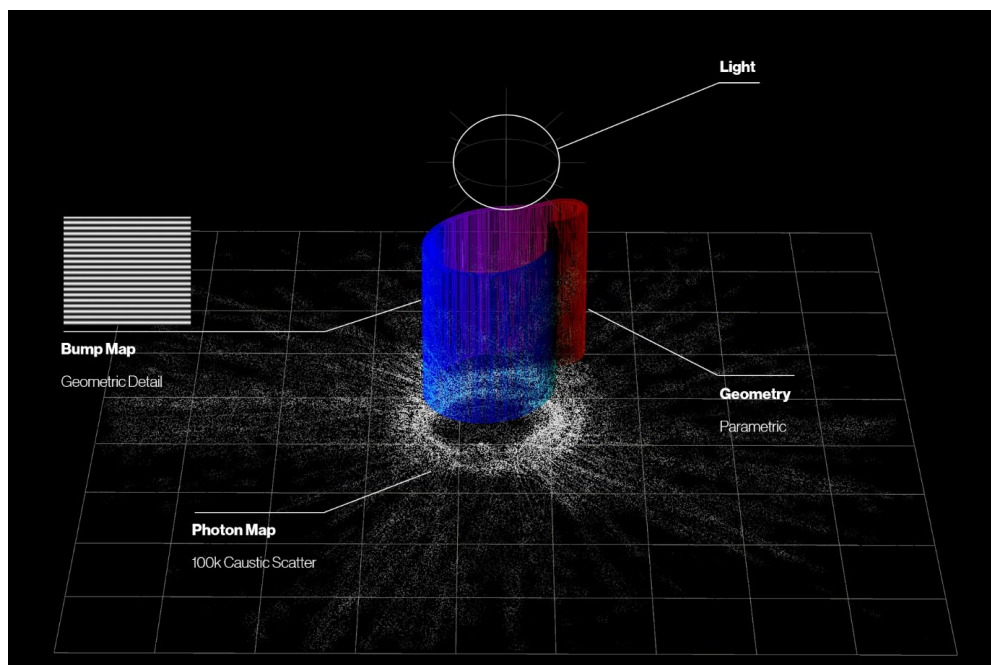


Figure 17. Creation of caustic photon map with raytracing through parametric glass geometry

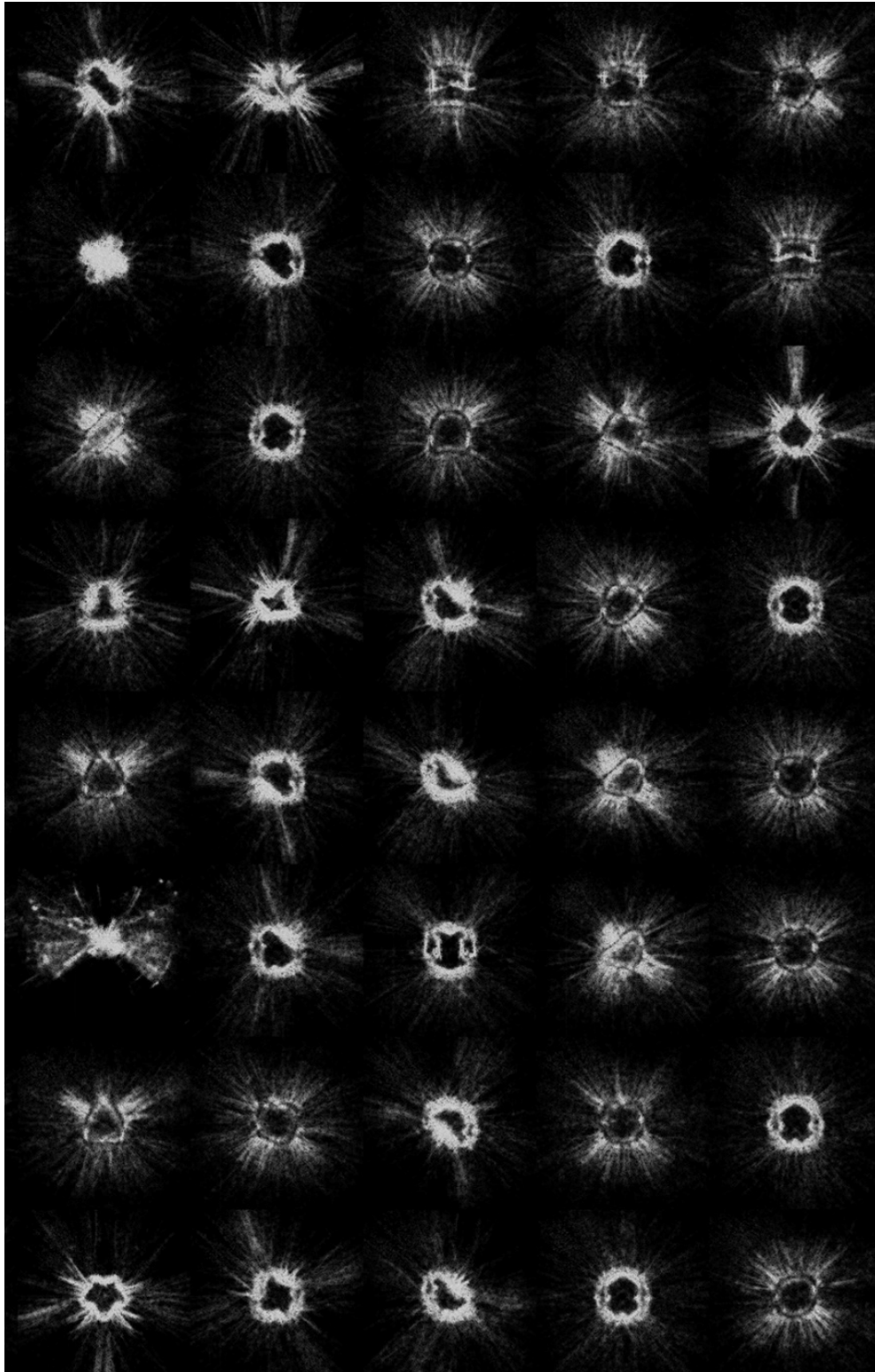


Figure 18. Selection of 40 out of 5,000 resulting caustic maps

Using a fixed light source, caustic light patterns were captured via raytracing and paired with the vectors describing the geometrical parameters. Using the software’s internal Mantra render engine, a fixed-point light source above the virtual glass object projected 100,000 photons onto the geometry. A resulting photon map was then saved as point data. To save time, the photomap was directly visualized, as an output image was generated with an OpenGL viewport screen capture of the point cloud. As training data for further machine learning, 5,000 geometries were processed and rendered, and their photomap capture images were stored with the corresponding geometry vector.

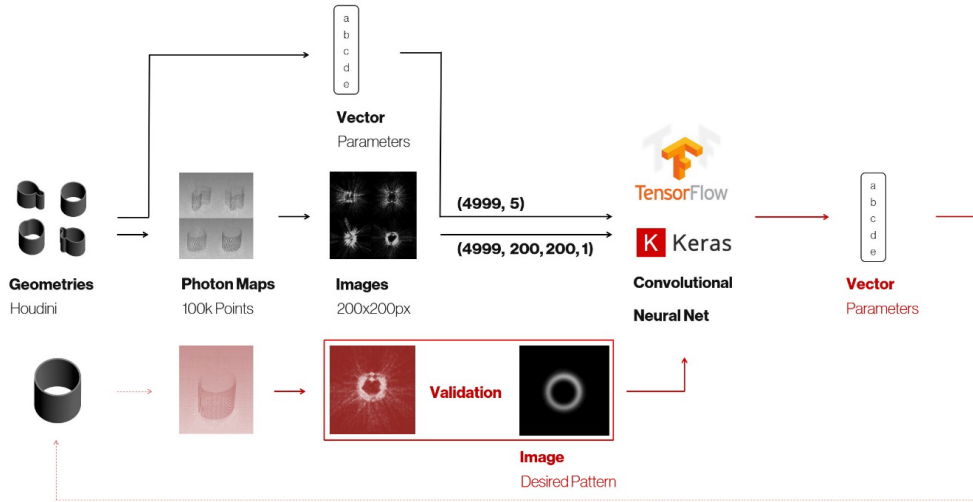


Figure 19. Geometry to caustic to neural net pipeline

4.2.4 Neural Network Creation

The goal of the machine learning process was to generate a neural net that would be able to match image data of caustic patterns with a geometry vector describing a shape that would most closely create the desired caustic pattern. For processing and prediction, a convolutional neural network (CNN) was chosen, as this network architecture has been successfully used for a variety of image-to-vector mapping problems (LeCun et al. 1989).

A variety of different networks were tested on the dataset. The networks were tested with 5,000 geometry vectors and their corresponding caustic image, with a training validation split of 30%. The first network architecture (Appendix NN1) consisted of a standard CNN with three Convolutional Layers, combined with Activation and MaxPooling, followed by a dropout and two Dense layers. In a second network architecture (Appendix NN2) the CNN model was combined with the pre-trained layers of the existing VGG16 Network. The VGG16 network (Simonyan and Zisserman 2015) passes images through a stack of convolutional layers, followed by fully connected layers. Custom flattening and dense layers

adapted the existing network. A third network architecture (Appendix NN3) was implemented as a simple convolutional layer with MaxPooling and flattening, followed by three dense layers.

4.3 Results

The resulting geometry pipeline was evaluated qualitatively by comparing input and output images. A series of seven images with a caustic pattern of an existing geometry and a series of three images with an abstract light shape were drawn and input to the best performing neural net architecture (NN3). The model had previously shown a mean absolute error of 0.1522 and a mean squared error of 0.046 in the validation step — no seeming correlation between the images was noticeable. Apparent features such as a hole, ring, or light point were not transferred visibly into the output.

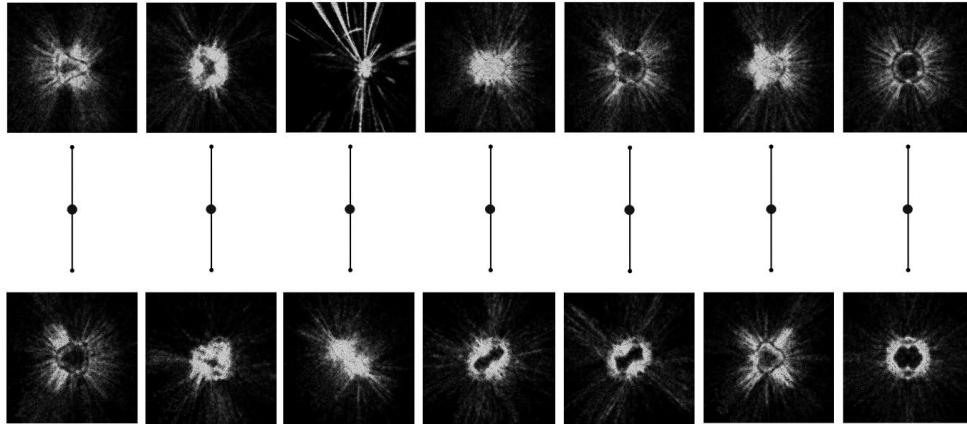


Figure 20. Input images (top row) were processed by the neural net. Output images (bottom row) resulting from the predicted geometry parameters

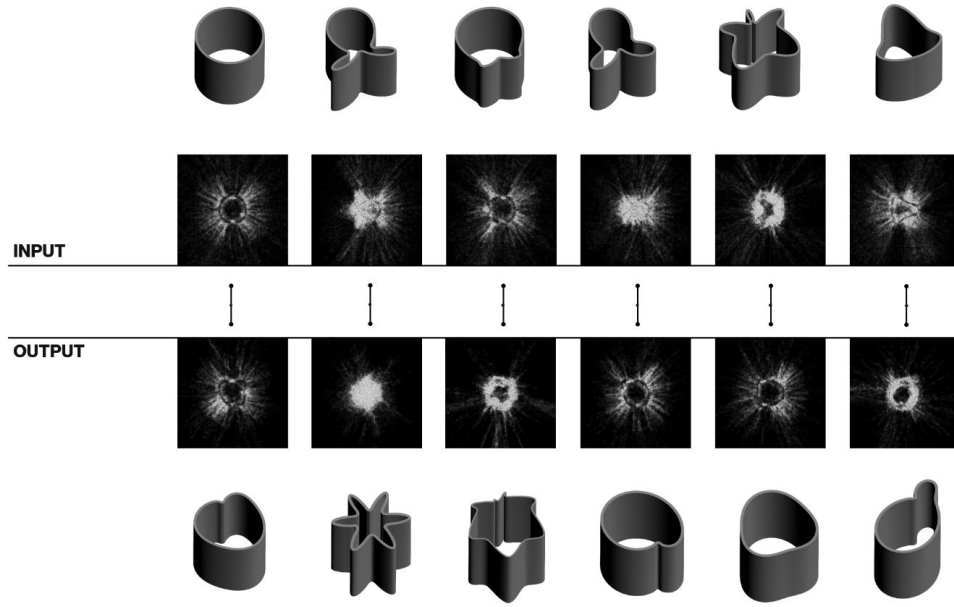


Figure 21. Input shapes (top two rows) with corresponding caustic image and output geometries (bottom two rows) with corresponding caustic images

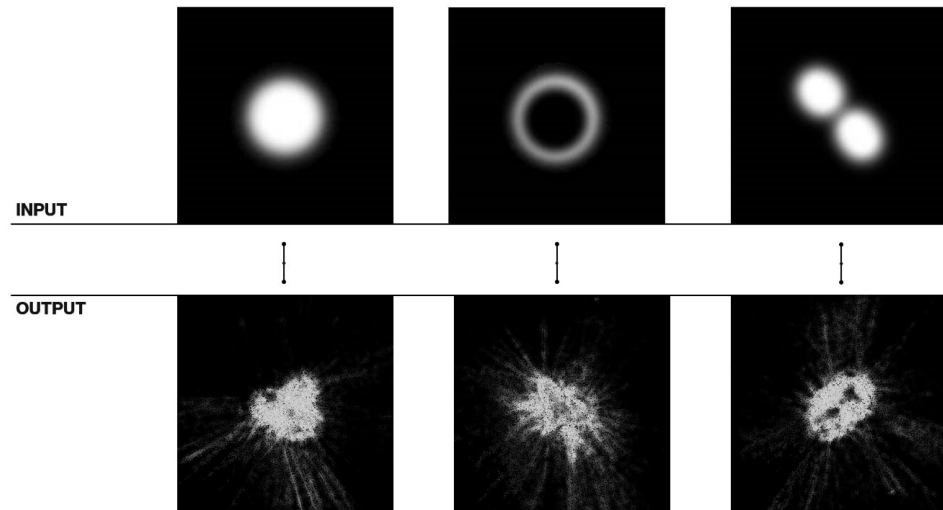


Figure 22. Abstract input caustic images (top row) and the processed output caustic maps based on the predicted geometry vector

4.4 Discussion

4.4.1 Sources of Error

Analysis of the result showed none to very little correlation between input and output images. Multiple sources of errors that could contribute to this were identified in the workflow. The first possible contribution was a limited dataset. Aggregated image libraries that are commonly used for image classification, such as the *ImageNet* Challenge, use 1.2 million images for training and 150,000 images for validation (“ImageNet, Large Scale Visual Recognition Challenge” 2017). Therefore, adapting useful networks for these large-scale image classification tasks to a data set of, in this case, 5,000 image/pairs with 3,500 training and 1,500 validation images, is prone to error.

Secondly, the geometric algorithm based on the Fourier basis included parameters (such as the period of the curve) that require integers, while other values (such as their corresponding offset values) operate with floating point values. Even though the input vectors were normalized into a 0 to 1 space, slight changes in a parameter, such as period, could lead to vastly different geometries when rounded and converted back into the input number range. A simpler and more linear model describing the geometries should lead to more predictable results.

Thirdly, sampling and validation could be further improved. The design space of the geometric parameters was sampled as a grid. More differentiated data gathering methods could lead to a better variation in the results across the whole design space. Instead of classifying the success rates of the results manually, a more accurate metric must be introduced. Noise and highly differentiated images as a result of the caustic reflections make comparing the resulting images very difficult. Using the Wasserstein distance (Solomon 2015) as a metric could enable a classification by matching and comparing the mass and density of the underlying photon distribution.

4.4.2 Contributions

This research implemented a novel parametric workflow for data creation and analysis by combining readily available software packages such as SideFX Houdini, Keras, and Tensorflow, with custom Python extensions. Fabrication-aware modeling of a shape library of 68’355 geometries served as the basis of the exploration. It could be shown how novel design tools can be implemented to explore highly differentiated and constrained design spaces. The proposed workflow could be further extended to allow for implementation in a variety of different design problems that can be distilled into the proposed input and output vectors. This research showed how machine learning could help designers approach novel

material systems through the inverse design problem to create previously unimaginable output.

4.5 Outlook

4.5.1 *Further Neural Net Development*

In the future, simpler design spaces and a more controlled linear geometry library will be implemented. Expanding the dataset to include at least 50,000 images for training would likely improve the accuracy of the system. Alternative validation and processing parameters should be explored further. Using a raster, instead of a vector, image of the base contour could allow for the use of Pix2Pix (Zhu et al. 2017) to matching boundary curves with corresponding caustic patterns. Comparing the difference between input geometries in addition to the output caustic photon map has to be explored. The difference between geometric difference and difference of caustic patterns could be analyzed and correlated. Furthermore, since the light scattering largely depends on the surface texture, the bump map used to create the scattering should be calibrated with existing physical models and might be derived directly from 3D scans of existing printed glass to more accurately reflect and predict the results.

4.5.2 *Design Implications*

Both material properties and overall geometry have a direct impact on the object's behavior in light. This research does not emphasize the optimization of a rigid design problem but rather how a digital toolset can explore the design space of a highly articulated fabrication process. On an object scale, small changes in geometry can result in a largely differentiated caustic pattern. Scaling up the 3D printed glass structures requires an in-depth study of lighting properties. Intricate geometrical and material differentiation can prevent glare and direct the focus of the light to pass through the object. Glass surfaces that could provide shading effects via geometric patterning, avoiding glare, and reflecting sunlight, while cultivating well-lit spaces. The inherent relationship with light proposes a new design workflow that allows for the design of both glass geometry and caustic pattern alike.

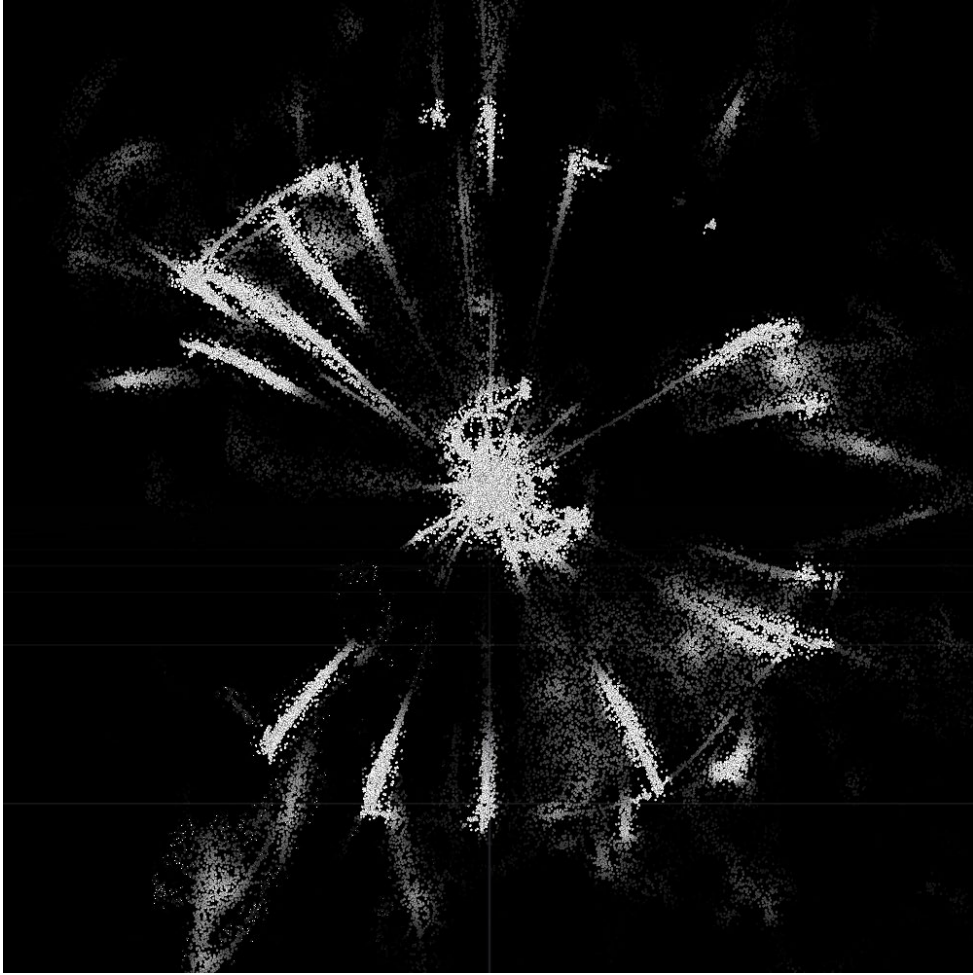


Figure 23. Closeup of photon map with 10'000 scattered points

5 Structural Shading²

Ramon E. Weber^a, Caitlin Mueller^b, Neri Oxman^a

^a Mediated Matter Group, MIT Media Lab, Department of Architecture and Urban Planning

^b Digital Structures Group, Department of Architecture and Urban Planning

5.1 Abstract

Shading fin systems are often secondary add-ons to building envelopes rather than intrinsic structural elements. However, there is significant performance potential in using linear fin-like elements to perform both structural and shading roles, especially in roof and facade structures such as gridshells and exoskeletons. This approach can lead to the reduction of both embodied and operational energy, through efficient structural design, combination of functions, and performance-oriented daylighting control. This research outlines how computational optimization strategies and design space exploration methods can be combined with both structural and energy simulations to create high-performing structural shading elements. The inherent link of form, material, and environment is presented as a framework for both gridshell façade and roof structures. We create an integrative workflow by pairing environmental data with qualitative architectural constraints.

By designing and optimizing building elements to perform structural and shading roles simultaneously, we can unlock design potential and consolidate function, leading to improved environmental performance and a new architectural vocabulary. Our results show how leveraging the geometric complexity offered by novel digital design methods and fabrication techniques can reduce the embodied energy of structures significantly. Furthermore, our computational methods can be used to develop passive structures that react to opposing forces of local climate; creating shade in summer, while maximizing solar gains in winter.

Keywords: Building performance simulation, structural optimization, embodied energy, shading, design space exploration, multi-objective optimization, architectural geometry.

² A version of this chapter is currently under review as a paper manuscript.

5.2 Introduction

The built environment is one of the main contributors to climate change. In the United States alone, building-related emissions account for 40% of carbon emissions in the atmosphere today (World Green Building Council (WGBC), IEA, and UN-Environment 2018). With the number of households expected to increase by 12.2 Million in the next two decades (McCue 2018) architecture faces the enormous challenge of delivering carbon neutral buildings. Tackling this global challenge requires rethinking current design methodologies and workflows to include energy and carbon as main design drivers. The embodied energy of a structure is a key factor in the creation of more sustainable structures. Reducing it requires careful selection of building materials, reduction of material, and an increase in a building's lifespan. In architectural practice, building performance is for the most part significantly determined in early stages of design (Aksamija 2015), where considerations of architectural, structural, material, and energetic performance are often detached from one another or excluded. While architecture and engineering design teams regularly rely on computational methods for both structural optimization and energetic analysis of structures, it is vital they are used in combination with one another. We aim to demonstrate how bridging the disciplinary gap and helping to visualize and integrate various performance metrics into the design and decision-making process can lead to more efficient structural systems.

This research combines environmental parameters with structural optimization to create an integrative design workflow. In the creation of roof and façade structures with linear fin-like elements, we identify the potential to combine goals in terms of shading and structure toward more efficient overall systems. A series of digital experiments are used to evaluate the performance in dimensioning of beam members of waffle shell structures with solar radiation and the energetic performance of its space. We analyze the benefits of multi-material systems, overall architectural geometry, and orientation of individual members across scale in both gridshell façade and roof structures.

Integrative design approaches have been present throughout architectural history and excel where architects apply a deep understanding and control of structure and materiality. The work of Jean Prouvé, combined highly efficient structural systems of prefabrication in metal and wood to create lightweight modular buildings. For instance, the house for Abbé Pierre 1954 “Maison des Jours Meilleurs” in Paris, (LUMA 2017) where the multifunctional loadbearing steel core is combined with lightweight façade elements. In the 1960 Milan Triennale in the Palazzo dell'Arte, Italian architect Luigi Moretti (Imperiale 2018) demonstrated the usage of parametric optimization methods to derive optimal forms for the design of stadiums. Eladio Dieste combined structural principles with daylighting in roofscapes such as the CEASA factory hall in Porto Alegre, Brazil in 1970 (Anderson, Dieste,

and Hochuli 2004). The brothers Aladar Olgyay and Victor Olgyay formulated the first geometric methods and rulesets for architectural geometry and solar control (Olgyay and Olgyay 1977). The buildings demonstrate how structural components can be lighter and reduced to their essential parts when the design considers holistic parameters and workflows.

Computational optimization techniques have been widely applied to building systems envelope and energetic design problems (Evins 2013). However, design decisions and performance in the built environment are often difficult to formulate mathematically. New computational workflows are needed to allow goals such as structural efficiency, embodied energy, or cost to be paired with qualitative architectural constraints (Mueller and Ochsendorf 2015). Additionally, assessing the performance score of a design, by identifying and comparing Pareto fronts in these multi-variable design spaces can pose significant challenges (Brown, Tseranidis, and Mueller 2015).

Custom software, such as ParaGen (Turrin, Buelow, and Stouffs 2011), offer the possibility to link simulation and generative design tools with genetic algorithms to breed and generate novel design options integrating both structural and environmental concerns (Turrin et al. 2012). In contrast, this research investigates integrative structure and energy workflows that can be merged into existing architectural design tools. Furthermore, even though FEA analysis was performed, only the underlying scaffold spaceframe structure and not the shading devices itself were considered in the structural evaluations during the optimization.

Shading systems and louvers have a big impact on the thermal performance of a building. Optimal dimensioning allows for shading during warm periods to prevent overheating, while allowing for sunlight inside to help with heating during colder seasons. Multiple generative systems to aide in the design of shading devices with improved thermal performance in any location have been proposed (Sargent, Niemasz, and Reinhart 2011; Manzan 2014; Marsh 2003). The outputs resulted in both optimal shading geometries for louver systems and validated energy models, highlighting the building performance benefits. However, the shading geometries were only materialized without loadbearing function (Bechthold et al. 2011).

It has been investigated how freeform shading and lighting systems from planar quads should be optimized to block light from given sun angles while maintaining certain geometric properties (Jiang et al. 2013; Wang et al. 2013). Geometric flexibility and stability are considered in the creation of torsion-free structures from planar strips but remain constrained to the model-making scale.

Based on Erwin Hauer's screen designs, Omidfar analyzed how parametrized and geometrically complex shapes could be used as performative shading devices (Omidfar

2011). Variability of form was coupled with solar radiation performance simulations and compared to traditional, fully glazed façades without a secondary screen. Even though used as a façade element, the structural and material properties of the Hauer screen were not considered.

On a building scale, representation such as Building Information Modeling (BIM) allow for limited parametric adjustments of window size and global geometry to be considered in multi-objective optimization workflows (Asl et al. 2014). Using variation in building geometries, multi-objective search can further be used to minimize the total building energy for a specific climate and urban context (Méndez et al. 2015).

The research presented in this thesis expands on the combination of parametric geometry with structural optimization and solar simulation techniques. Going beyond abstract geometric representations for structural and solar simulations, we work on a detailed architectural scale for both the façade and roof structures. Even though optimal shading geometries have been the subject of extensive research, their usage as structural systems has not been studied. Furthermore, in contrast to existing research, we aim to integrate materiality as a key factor in the digital design and optimization process.

5.3 Methodology

This paper outlines how tools from the environmental simulation domain are combined with structural analysis methods and parametric modeling techniques. As an initial step, three parametric models, a roof, a shell and a diagrid structure (Figure 24), were generated in the architectural CAD software Rhino and its integrated node-based scripting platform Grasshopper with the usage of custom Python components. The specific software setup is widely used in the architectural design community, making the methods proposed easily transferrable from research to industry.

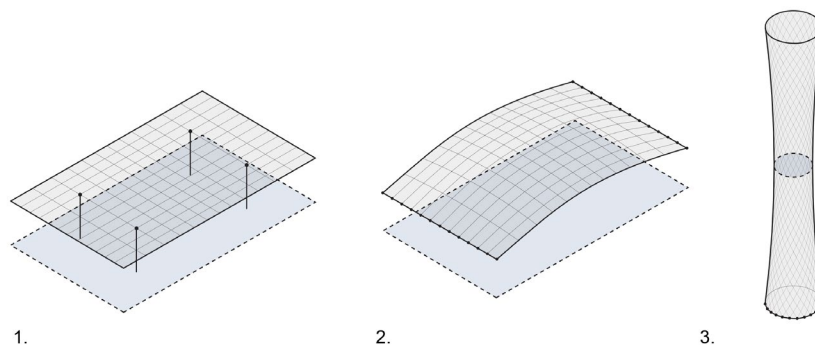


Figure 24: Architectural typologies tested in the digital experiments: Freestanding roof (1.), gridshell with two open sides (2.), gridshell façade (3.).

5.3.1 Design and Optimization Workflow

For each of the three models, representing different architectural typologies, a series of four experiments create a range of test cases (Figure 25)— a freestanding gridshell roof with column supports (A, B), a building-integrated gridshell with two open sides (C), and a structural gridshell façade (D).

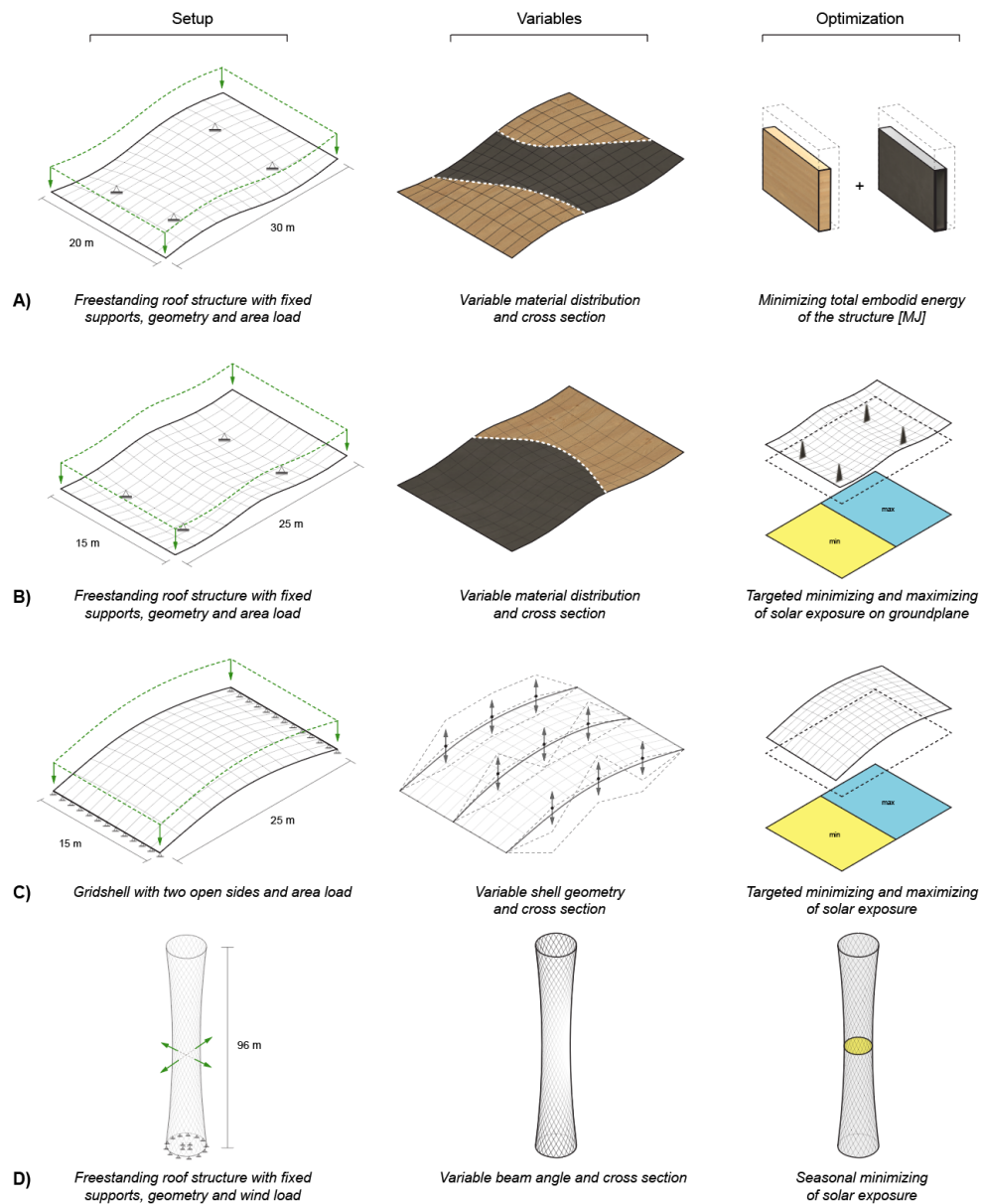


Figure 25: Description of digital experiments A-D with their setup, variables and optimization parameters.

The three models have variable base geometries and a more detailed structure superimposed; additional parameters to detail the structure's geometries were added and can be controlled. In a feedback loop (Figure 26), the geometric model is constructed, optimized structurally, and analyzed for its environmental performance. A combined performance score then is used for iterative optimization of its environmental performance. Environmental performance, in this case, was a metric derived from the annual solar radiation on a predefined sensor surface beneath the structure. In the case of the façade, the sensor surface was placed on the floor slab in the interior of the building.

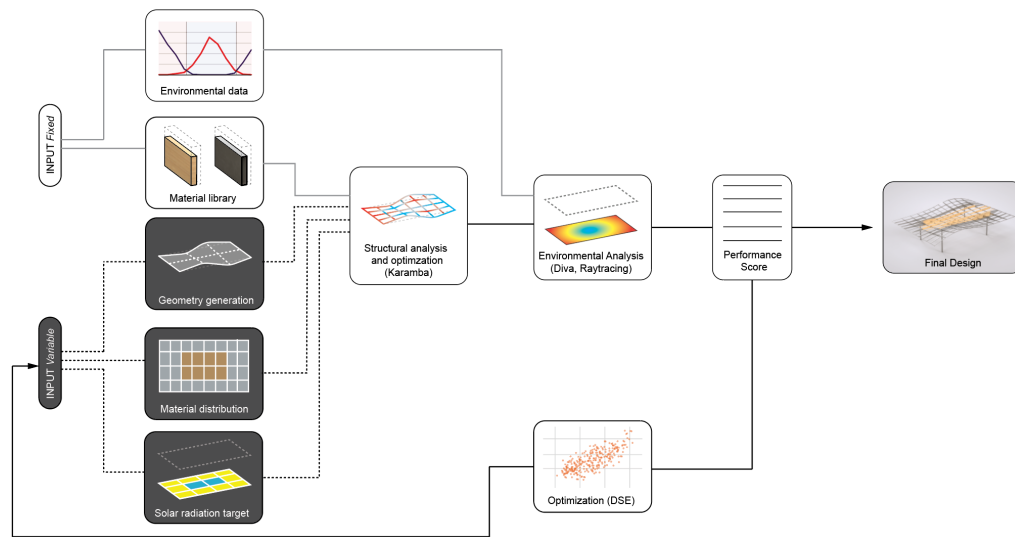


Figure 26: Overview diagram for iterative computational design workflow, utilizing structural and environmental performance for multi-objective optimization.

The models were parameterized in low resolution, minimizing the number of parameters while maximizing the possible variability of the geometry. In the first of three steps, the models were generated from a series of control points, defining the structure's surface. The positions of the control points served as variables for the optimization. The boundary curves defined by the control points were then used to create a grid, defining the location of the beams. The design space exploration framework (DSE) was used to sample, record, and optimize design iterations (Brown et al. 2016). Randomized and Latin Hypercube sampling was used to provide an initial sense of the design space. Since there were always a series of input variables for geometry and material selection, a multi-objective optimization method had to be used. As implemented in DSE, we utilized the NSGA-II multi-objective optimization algorithm (Deb et al. 2002), a genetic algorithm, to iteratively create new generations of higher-performing solutions.

5.3.2 Methods for Structural Optimization

The parametric structural design tool, *Karamba* (Preisinger and Heimrath 2014), is used as the structural component in the parametric feedback loop. Its implementation in Rhino allows for an interface with environmental and geometric constraints. The internal function of cross-section optimization was used to choose between a select range of possible dimensions for the structural parts. Variable hollow rectangular tube steel and solid rectangular timber cross sections are used in the digital simulation, as described in Table 4.

	Variance Height [cm]	Variance Width [cm]	Thickness [cm]	Elastic Modulus [kN/cm ²]	Shear Modulus [kN/cm ²]	Density [kg/m ³]	Embodied Energy [MJ/kg]
Steel	5 – 200	5 – 20	1.0	21000	8076	7850	24.4
Timber	10 – 200	2 – 10	Solid	1050	360	530	7.4

Table 4: Material definitions used in the structural simulation.

An adaptation of the level set method was used for the material selection across the roof geometries (Figure 27). The two materials, timber and steel, are assigned to different members of the gridshell via a control surface with nine control points. This allowed for minimization of the number of variables input to the optimization while retaining a wide variability and control. The roof structures have a gravitational loading and a constant area load across the surface of 5 kN/m² applied. Supports are defined as hinge supports.

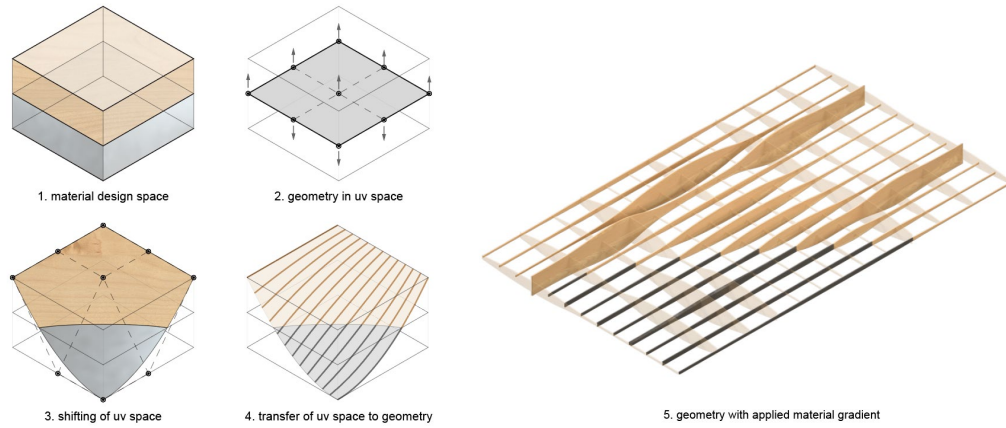


Figure 27: Level set method for adaptive material selection.

5.3.3 Methods for Environmental Analysis

Two methods for the analysis of lighting were used. First, simplified direct solar vectors (Duffie and Beckman 2013) were implemented in the Grasshopper and Rhino environment via custom Python components. In combination with internal occlusion methods, it allows for a fast and responsive simulation. Sun path rays during predefined times throughout the year were scattered on a base mesh surface and intersected with the simulated geometries. This primitive raytracing method was used in experiment B and created a very fast latency (19 ms for an annual calculation on a standard desktop computer) to give initial predictions of the shading properties. More accurate results from experiments C and D are given by annual solar radiation analysis in the experimentally validated light-backward raytracer *Radiance*, that is utilized via the DIVA (J A Jakubiec and Reinhart 2011) integration in the Rhino and Grasshopper environment. Sending information back and forth to the *Radiance* engine requires several seconds, making this option unusable for more real-time design experience. Because of the raytracing methods in *Radiance*, increasing resolution or variation in geometric features of the shading gridshell makes almost no difference in render time, only in the resolution of the base grid. The environmental simulations were conducted in virtual Boston, MA USA. Heating and cooling periods were adapted from Reinhart for the seasonal simulation in experiment D (C. Reinhart 2014), as outlined in Figure 28.

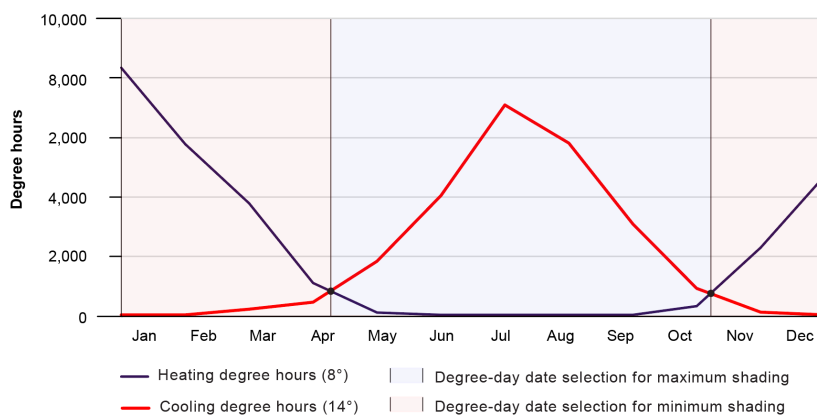


Figure 28: Degree day selection, as adapted from Reinhart (C. Reinhart 2014) for Boston: April 25th, ordinal date (od) 115, to October 21st, od 294, summer solstice June 20th, od 172.

5.4 Results

5.4.1 Experiment A: Adaptive Materiality for Lower Embodied Energy

The range of the cross-section dimension search has a significant impact on the overall weight and embodied energy of a structure. Figure 29 shows how adapting cross-section dimensions throughout every element in the whole structure can result in a waffle slab utilizing only 25% of the material of a single optimized cross-section. A smaller allowed search domain will present over-dimensioned structures that use fewer different elements. A wider search domain will pick dimensions much closer to their force requirements and result in a greater variety of components.

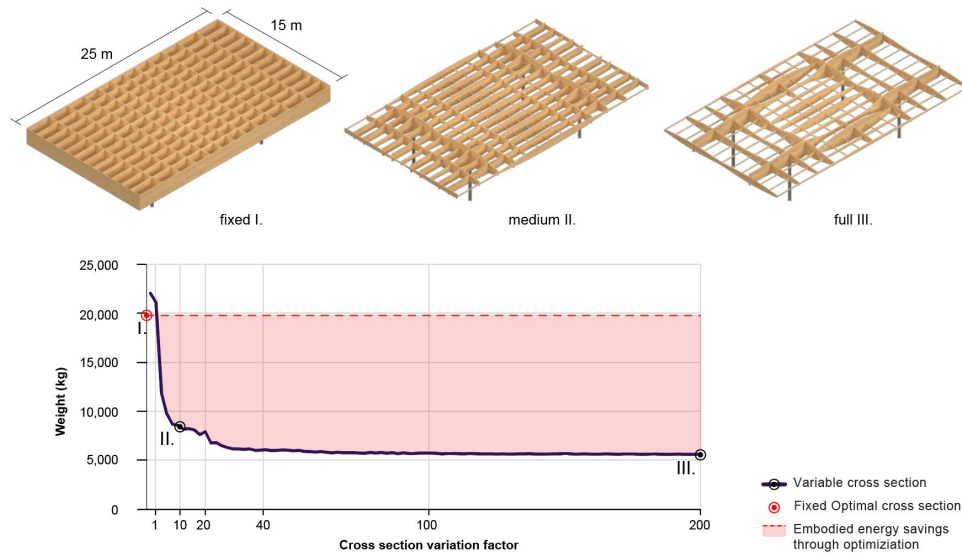
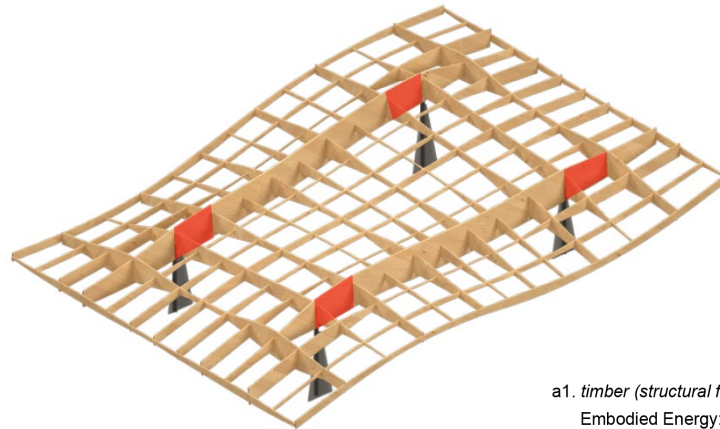
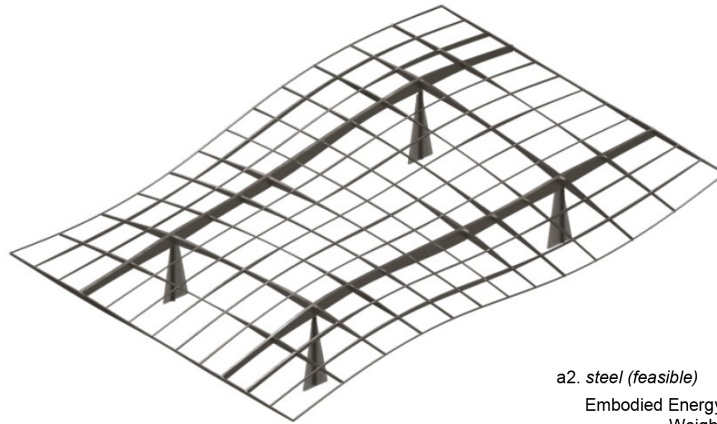


Figure 29: Cross-section selection range in relation to the weight of the overall structure.

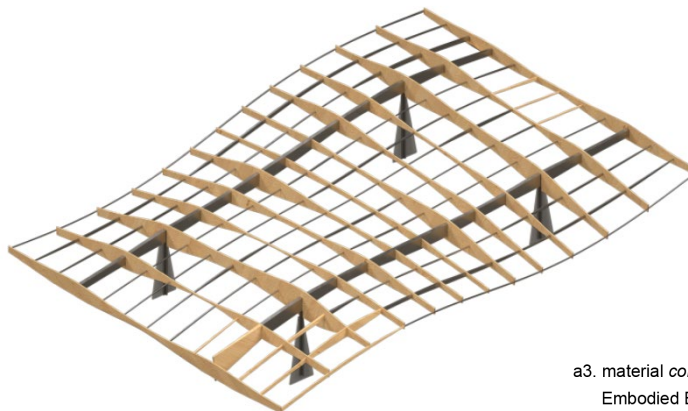
We expand this variability to adaptive material distribution as shown in Figure 30. The experiment shows a larger waffle slab spanning 30 x 20 m with four column supports. Its slightly undulating geometry is fixed as a design input and the material distribution variable, as in the described level set method. The all-timber solution (Figure 30 a1.) results in failure, while an all-steel solution (Figure 30 a2.) results in a waffle roof with high embodied energy. We therefore optimize for the lowest embodied energy solution while retaining structural stability, by variation of the material distribution. This creates a roof structure (Figure 30 a3.) with a performance gain in terms of embodied energy of almost 30% compared to an all-steel solution. A plot of the sampling in the design space exploration (Figure 31) reveals a wide range of possible solutions that perform better or worse than the all-steel solution.



a1. *timber (structural failure)*
 Embodied Energy: 91,023.5 MJ
 Weight: 12,300.5 kg



a2. *steel (feasible)*
 Embodied Energy: 349,275.5 MJ
 Weight: 14,314.6 kg



a3. *material combination (feasible)*
 Embodied Energy: 240,016.7 MJ
 Weight: 13,868.4 kg

Figure 30: Visualizations of input for structural simulation as fixed mesh with four supports, materialization in timber (a1.) with failing cross sections in red, and all-steel solution (a2.), final material combination (a3.).

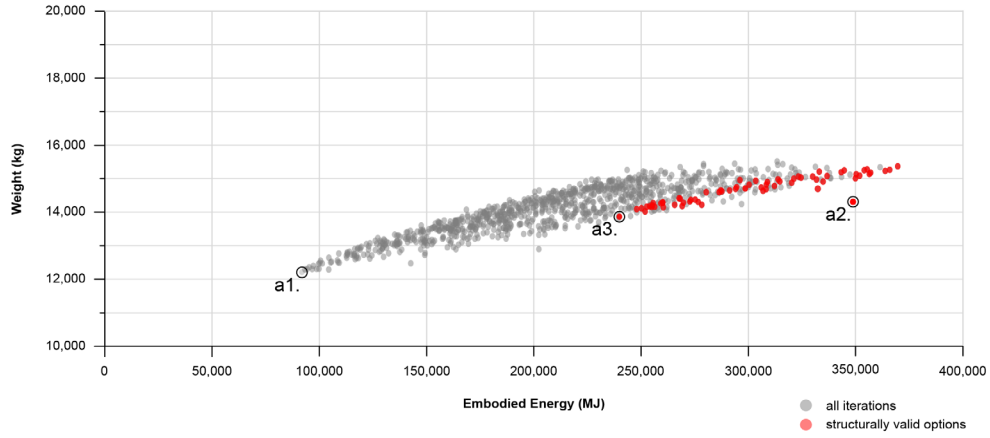


Figure 31: Sampling of design space with visualized weight and embodied energy of solutions.

5.4.2 Experiment B: Material Optimization for Solar Radiation

The second experiment optimizes material selection towards the desired shading goal (Figure 32). We assume a waffle gridshell with a fixed geometry, supported by four columns. Variations in material distribution create structures with very small cross-section in steel and cross-sections of large depths in timber; cross-section is directly related to the shading properties of the gridshell. Optimization for maximum solar radiation results in an all-steel structure (Figure 32 b2), while optimization for minimum solar radiation results in an all-timber structure (Figure 32 b1). With multiple radiation targets, we can create a structure that automatically adapts between maximum and minimum shading (Figure 32 b3). The performance score is derived from the difference of the sum of all rays intersecting the roof geometry.

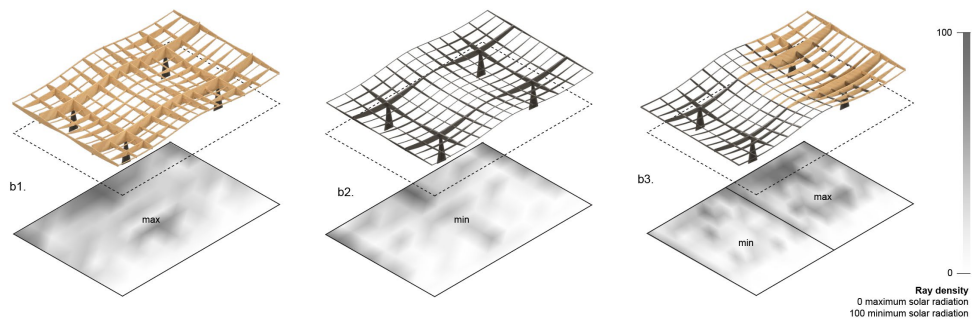


Figure 32: Material optimization towards a shading goal: Maximum shading (b1.), minimum shading (b2.) and area selective shading (b3.).

5.4.3 Experiment C: Geometry Optimization for Solar Radiation

We can use geometric features to create areas with more or less shading. We optimize cross-section dimensions on variable input geometries. Concave and convex features of the gridshell result in smaller and larger dimensioned cross-sections, which have implications in the environmental performance. Utilizing the same boundary conditions, we can generate geometries that perform for certain solar radiation target distributions. The results of the optimization (Figure 33) show two roof gridshell geometries that perform best towards a solar radiation target of minimum and maximum shading of a specified area.

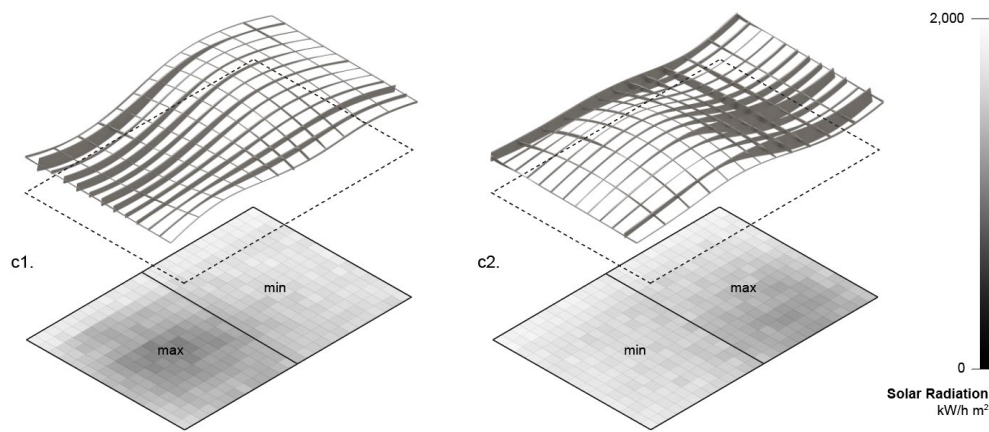


Figure 33: Geometric variation is achieved through the vertical movement of control points. Optimized mesh for maximum shading on the left sensor surface (c1.) and the right sensor surface (c2.).

5.4.4 Experiment D: Seasonal Optimization for Facades

Façades have conflicting shading requirements. In a climate such as Boston, winters require substantial heating while summers require cooling of a building interior to retain comfort. Therefore, global shading will have a negative impact and require more heating in colder times of the year. The simulation setup uses a reinforced concrete core with floors spaced 4 m apart and a 96 m tall grid mesh as inputs, as described in Figure 34. In addition to the gravitational loading, a 2.5 kN/m² wind load from four directions is applied to a secondary load mesh across the surface. We utilize our level set method, but instead of adaptively changing the material we change the rotation of the beam members along the façade surface (in UV Space) before the cross-sections are optimized. Throughout the sampling iterations, the input values for the control surface for the rotational control are randomized, creating a variety of façade solutions.

A sensor surface is placed in the center of the building (Figure 34, 6.) to measure an annual daylight distribution. Additionally, as a reference, we measure the annual daylight without

the surrounding building. We extract the daily average illuminance in lux on the day of the summer solstice and the winter solstice.

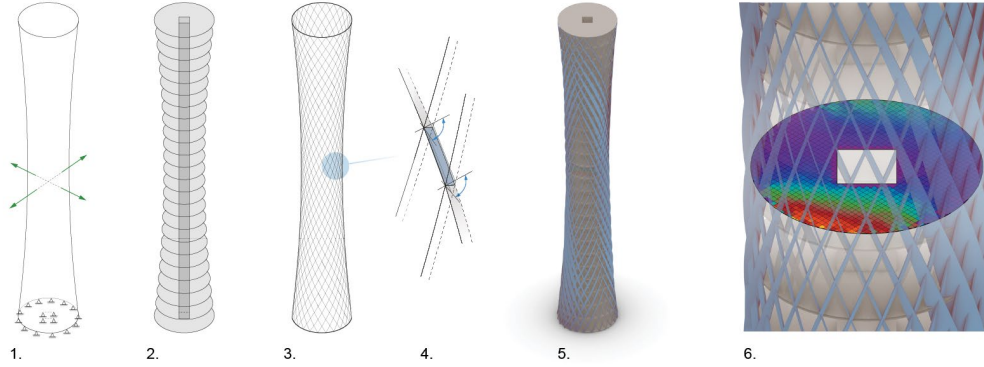


Figure 34: Façade optimization setup: Definition of loads and supports (1.), core (2.), diagrid (3.), rotation of beams (4.), dimensioning of beams (5.) and simulation of illuminance and solar radiation (6.).

The optimization function filters iterations that maximize the difference between winter luminance and summer shading. The goal is a façade design with maximum shading in summer and minimum shading in winter. For each iteration, the embodied energy is calculated from the volume of material used. Visual renderings of three samples are displayed in Figure 35. The scatter plot (Figure 36) shows detailed information about the façade iterations. The three-dimensional visualization reveals a positive linear correlation between measured light levels and embodied energy. The randomized design space exploration shows that daylight performance varies by up to 50% in the summer and 30% in the winter for the design space set by the geometric constraints. This is confirmed by the visualizations, as increased rotation of the façade elements requires larger dimensions in thickness and through that, creates more shading. However, our objective function mapping of the summer-winter difference reveals a range of performative solutions that even though similar in light distribution, vary significantly in their embodied energy.

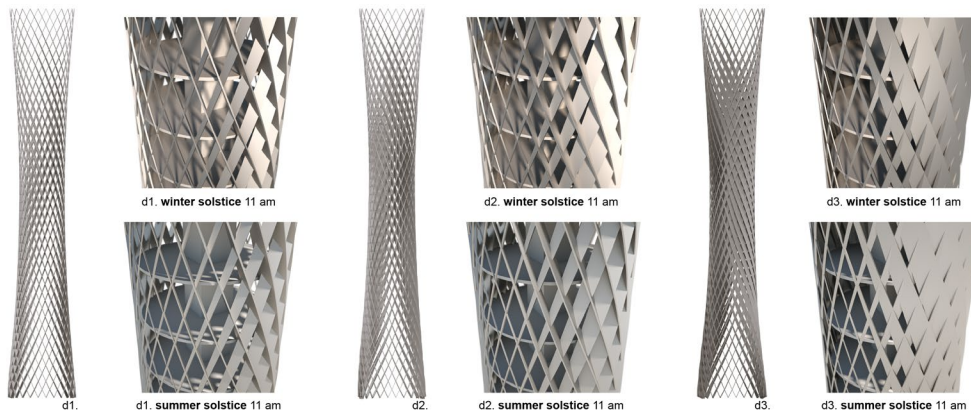


Figure 35: Sample façade iterations in elevation and closeup renderings at winter and summer solstices.

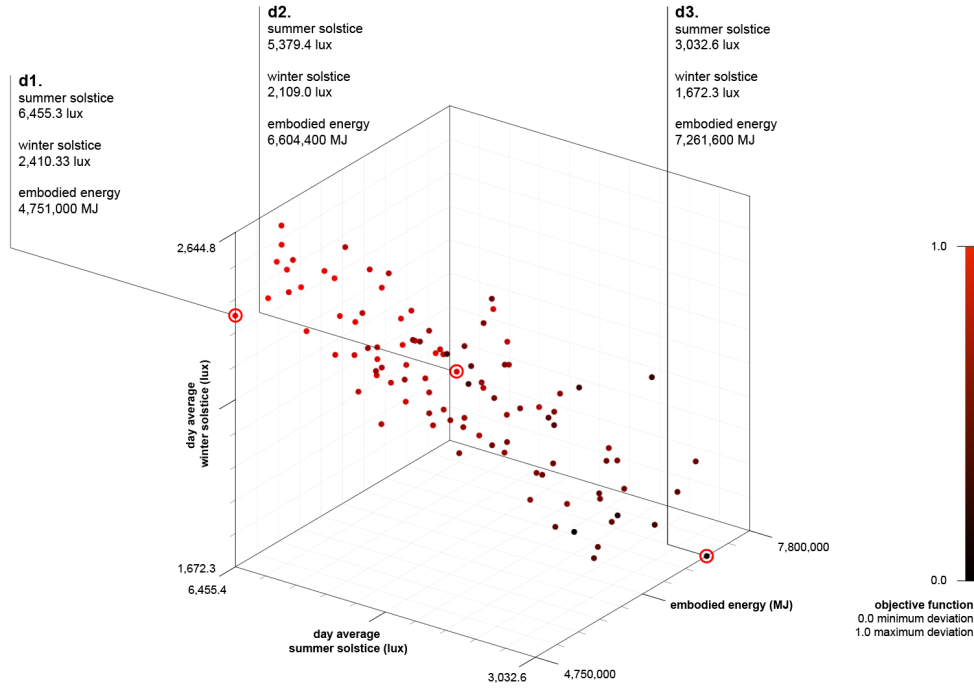


Figure 36: Summer and winter solstice daily average of luminance levels and embodied energy. The summer winter variance is the result of equation (1). Reference values were obtained by analysing the sensor surface without obstructing building geometry.

$$v_n = \frac{\text{summer solstice actual}_n}{\text{summer solstice reference}} - \frac{\text{winter solstice actual}_n}{\text{winter solstice reference}} \quad (1)$$

5.5 Discussion

As parametric models and generative geometric design processes yield almost infinitely variable options, it is important to create strategies on how to identify more performative design solutions. Interactive visualizations that display design variants, together with a performance score, are important to give the user an intuition of the design space. Furthermore, the creation of diverse design solutions and appropriate sampling strategies are necessary to fully explore a design space. Multi-objective optimization can be used to negotiate between a range of performance factors.

The formal repertoire of architectural geometry has expanded significantly in the last years. Numerous examples of highly complex geometries for envelopes and structures have been manufactured for high-end architectural projects. Even though geometrically complex architectural design is mainly motivated by aesthetic goals, it also provides a geometric

grammar and pushes the boundaries of bespoke manufacturing on a building scale. Our digital experiments show how this freedom of form and the creation of non-standard geometries, enabled by digital fabrication and planning solutions, can be leveraged to create more functional and performative design solutions.

The implementation of environmentally aware computational design methods, although technically feasible for many years, faces significant challenges in real-world implementations. The latency and low speed of optimization tools oftentimes creates non-intuitive workflows that are difficult to implement in existing practices (Jones and Reinhart 2019). Implementing different levels of simulation accuracy as shown in our environmental analysis solutions can help to mitigate this issue of latency and allows for designer feedback during early design stages. However, for final building solutions, the usage of validated (slower) simulation tools is a requirement.

Through visualization techniques of both datasets and geometry, we enable an exploration of the implication of design decisions. User comfort, daylight, structural performance, and embodied energy can be compared side by side and the helpful tradeoffs can be identified.

5.6 Conclusion

Current trends in architectural design separate components with energetic function from the structure of a building. Shading systems are most commonly a secondary aestheticized layer added to a building envelope. We see an opportunity to create buildings with fewer materials by combining spatial and performative elements into multifunctional building components. Our research investigates how computational design methods, optimization, and solar analysis techniques can be used to create architectural systems that can be loadbearing while performing environmentally. It shows how multi-objective design exploration methods can negotiate between varieties of constraints to enable users to design structures that use fewer materials while performing better in terms of energy use and structural performance.

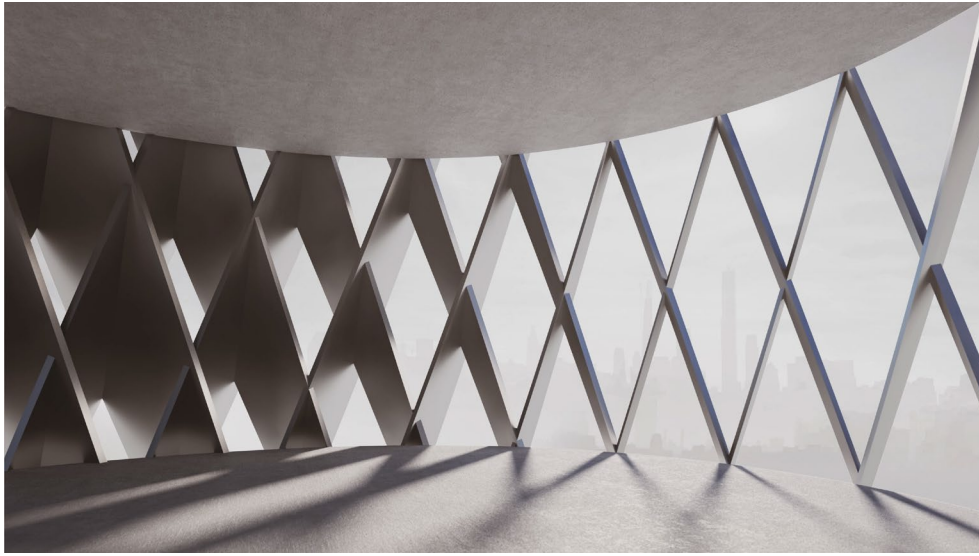


Figure 37: Interior rendering of iteration d1 with the façade letting light through at the winter solstice at 11:00 am.



Figure 38: Interior rendering of iteration d1 with the façade blocking light at 11:00 am.

The case studies have shown how geometric variability and complexity can have a substantial impact on the environmental performance of a structure. The roof studies show how increasing the variability of cross-sections that are dimensioned more closely to the forces required can result in significant material savings of up to 75%. Environmental performance in terms of daylight illuminance can increase by 50% with optimal placement of structural fins. The geometric variability showed how a large variety of designs could fulfill a similar lighting performance. This highlights that design variance does not have to be sacrificed for more performative design solutions (Figure 37, Figure 38).

We demonstrate how through the usage of a control surface for material selection or rotational control, the parameter space of complex geometric manipulations can be simplified and represented as variables with low dimensions. This allows for gradual adjustment and optimization of large geometric datasets.

The design of shading systems and louvers have a significant impact on the thermal performance of a building. Optimal dimensioning allows for shading during warm periods to prevent overheating, while allowing solar gains in winter to assist with heating. Furthermore, shading systems can prevent glare, increasing user comfort.

The case studies presented in this paper showcase the potential for implementing performance metrics into early-stage design workflows. They are limited by the constraints of parametric design with a predefined and fixed design space that does not allow for novelty during the optimization. For this more open generative grammar type, workflows that can implement and explore a variety of topologies should be explored. Additionally, more accurate energy analysis of actual heating and cooling gains, instead of simplified solar radiance and illuminance levels, should be integrated for more accurate predictions.

Freedom of form and full automation (e.g., in the manufacturing and processing of prefabricated wood structures) make material usage the largest expense in both cost and carbon, while processing and assembly remain cheap, creating incentives for the optimization of material.

We see material reduction strategies as a key to more sustainable building solutions that will require the implementation and adoption of new workflows to satisfy all architectural, structural, energetic, and performative constraints. New possibilities of digital fabrication and mass customization of building components must be considered for the design of novel performative structures. Further work could take on other architectural elements that go beyond fin systems. Implications for architectural design are manifold and the creation of holistic workflows forces interdisciplinary thinking back into early-stage design. This combined intelligence in the design process can create more efficient structures with higher performance.

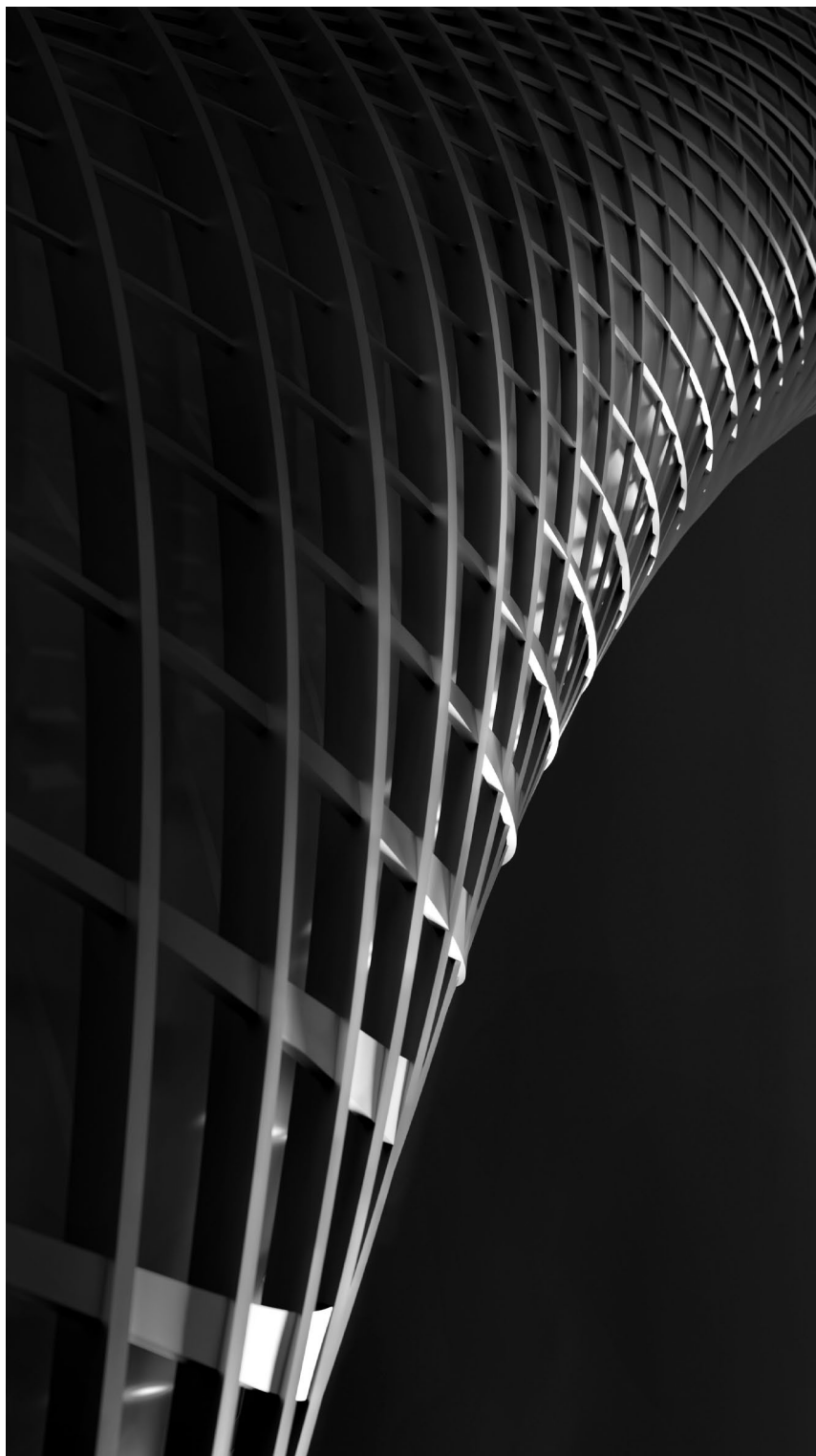


Figure 39: Rendering of the Structural Shading design framework applied to a façade geometry



Figure 40: Rendering of the Structural Shading design framework applied to a façade geometry

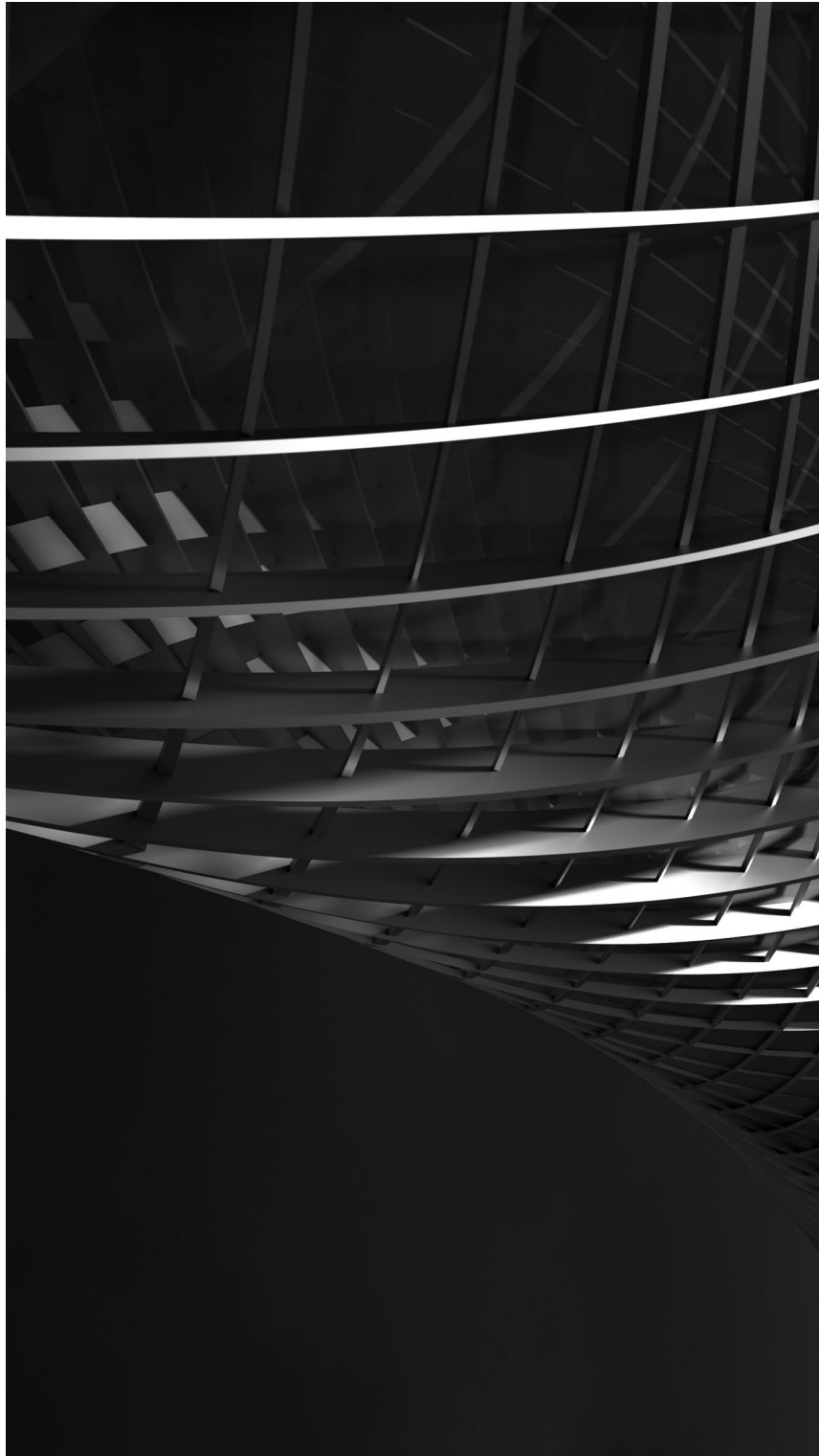


Figure 41: Rendering of the Structural Shading design framework applied to a façade geometry

6 Conclusion

In this thesis, I outlined different methods of relating geometry to light, along with the challenges and opportunities in accurately simulating digitally fabricated building components. The first chapter, *Photon Mapping of Geometrically Complex Glass Structures*, introduced the challenges with creating accurate light simulations. Light behavior through glass structures more complex than flat float glass cannot be simulated accurately with backward raytracing. 3D printed glass structures were used to evaluate the simulation performance of the photon mapping approach, an advanced light simulation method, on a building scale. A workflow for geometry capture and simulation of the 3D printed glass components was presented and digital simulations were compared with physical replicas of the experiments, as data pairs. Experimental setups with artificial and natural light demonstrated that photon mapping excels at simulating light behavior, with some limitations. Interior light levels and caustic light patterns could be predicted reliably, but some problems were noted in predicting glare and scattered light from the glass objects themselves.

The second chapter, *Programmable Caustics*, showcased the creation of novel parametric workflows for geometry definition and analysis. Robust enough to handle large datasets of tens of thousands of geometries, an automated process created photon maps for each geometric iteration. Design space exploration methods were used to navigate the multidimensional constraints of the large datasets. This manifold of data further allowed us to include machine learning algorithms into the design production of novel material systems and enable the inverse modeling of light behavior.

Moving from smaller-scale refractive objects to the building scale, light was used as a design parameter for the creation of *Structural Shading* systems in the third chapter. A new workflow combining geometry creation with solar and structural optimization techniques was proposed. The light simulation techniques allowed us to imagine multifunctional building components that combine solar (shading) performance with structural properties. Through a series of digital experiments, digital fabrication was shown to enable geometric complexity and significantly reduce material usage. Furthermore, by including real-world architectural materials such as timber and steel into the simulation and introducing methods of adaptively changing material distributions throughout a structure, the structure's embodied energy can be reduced substantially.

This unlocks new design opportunities in utilizing validated environmental simulation techniques as a design tool. We see how results from digital simulations can inform design decisions to create more performative spaces and structures. This contributes to a

transformation in the narrative of sustainable design — the environment and physical materials can be form-givers, rather than constraints. The methods show how machine learning and optimization can not only be used to achieve engineered efficiency but also as part of a creative workflow. They can be used to explore large design spaces and are key in designing with complex material systems.

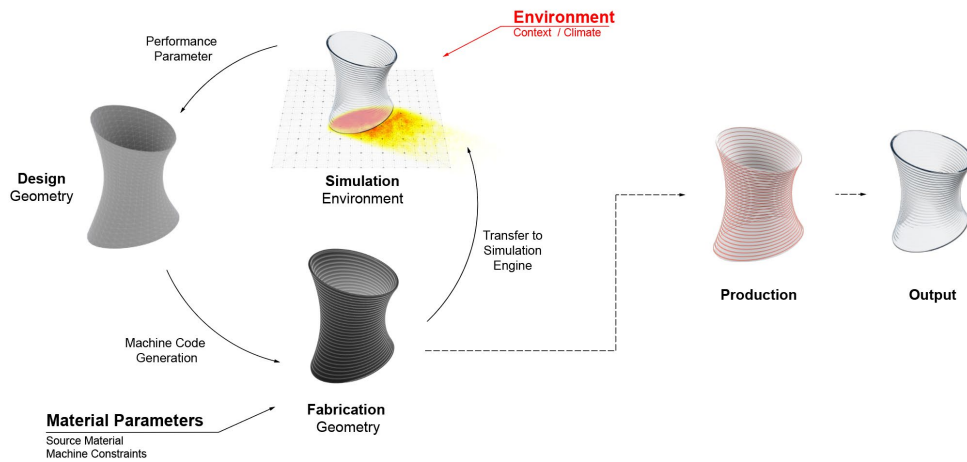


Figure 42: Relationship between physical and digital geometry during the proposed manufacturing process.

Bringing materiality into digital design workflows enables the physical domain to be represented highly accurately with virtual means. Validation and comparison to physical experiments create simulations with spatial implications that are no longer purely abstract. Looking at experimental manufacturing technologies in additive manufacturing (such as glass 3D printing) and non-standard digital fabrication, the simulation methods reveal their potential in creating performative building components and more material-efficient structures (Figure 42).

I explored how interdisciplinary tools and frameworks can be transferred to a design domain to create structures on an architectural scale. Specialist geometric modeling tools borrowed from the film and special effects industry, such as Maya (Autodesk 2020) and Houdini (SideFX 2020), offer new design freedom. Design space exploration techniques and machine learning algorithms can be used to leverage the parametric geometry workflows. Furthermore, there is room for further exploration by including engineering analysis tools and letting them interface with architectural production toolsets.

We see how different levels of accuracy, both in geometric representation and simulation accuracy, are needed to inform design across stages. Low-resolution raytracing techniques inside a design tool with low latency have different applications from high-resolution photon

mapping that accurately predicts light levels. They can be both valid tools, but each must be deployed in different situations.

Geometric abstraction remains an important factor in design production. Modes of low-resolution representation allow for fine control of parametric models while variable parameter numbers are kept to a minimum. This restriction allows for the successful use of optimization methods.

Fabrication-aware computation and new ways of interfacing parametric design solutions with digital simulation could enable the built environment to respond to challenges of the future. The methods can not only be used to assess existing manufacturing technologies and predict their impact but also to guide their development. Future work could address this and take real-world construction methods and assembly into account. Adaptive multi-material workflows could create more efficient structures across scales.

Accurate simulation of 3D printed glass can enable the production of future components on an architectural scale and could be applied to the development of novel Fresnel lenses and light redirection devices. Working with natural sunlight and local climate creates both a spatial and temporal dimension to the design, enabling adaptive structures that respond to the forces of nature.

7 References

- Aksamija, Ajla. 2015. "High-Performance Building Envelopes : Design Methods for Energy Efficient Facades." *Advances in Building Energy Research* 10 (2): 240–62.
- Andersen, M, and J deBoer. 2006. "Goniophotometry and Assessment of Bidirectional Photometric Properties of Complex Fenestration Systems ." *Energy and Buildings* 38 (7): 836–48.
- Anderson, Stanford, Eladio Dieste, and Stanforde Hochuli. 2004. *Eladio Dieste: Innovation in Structural Art*. Princeton Architectural Press.
- Artec3d. 2020. "Artec Leo 3D Scanner." 2020. <https://www.artec3d.com/portable-3d-scanners/artec-leo>.
- Asl, Mohammad Rahmani, Michael Bergin, AdamMenter, and Wei Yan. 2014. "BIM-Based Parametric Building Energy Performance MultiObjective Optimization." *32nd ECAADe Conference* 224: 10. <http://autodeskresearch.com/pdf/bimparametric.pdf>.
- Autodesk. 2020. "Maya." 2020. <https://autodesk.com/maya>.
- Banham, Reyner. 1969. "Architecture of the Well-Tempered Environment." University of Chicago Press.
- Bechthold, Martin, Jonathan King, Anthony Kane, Jeffrey Niemasz, and Christoph Reinhart. 2011. "Integrated Environmental Design and Robotic Fabrication Workflow for Ceramic Shading Systems." *Proceedings of the 28th International Symposium on Automation and Robotics in Construction, ISARC 2011*, 70–75. <https://doi.org/10.22260/isarc2011/0010>.
- Benjamin, David. 2017. *Embodied Energy and Design: Making Architecture between Metrics and Narratives*. Lars Müller Publishers.
- Block, India. 2018. "Robots Complete Span of 3D-Printed Bridge for Amsterdam Canal." *Dezeen.Com*, April 2018.
- Brown, Nathan, John Ochsendorf, Caitlin Mueller, and J. de Oliveira. 2016. "Early-Stage Integration of Architectural and Structural Performance in a Parametric Multi-Objective Design Tool." In *Structures and Architecture*, 1103–11. CRC Press. <https://doi.org/10.1201/b20891-152>.

- Brown, Nathan, Stavros Tseranidis, and Caitlin Mueller. 2015. "Multi-Objective Optimization for Diversity and Performance in Conceptual Structural Design." *Proceedings of the International Association for Shell and Spatial Structures (IASS) Symposium "Future Visions,"* no. 20: 1–12.
<http://digitalstructures.mit.edu/files/2015-09/ncb-iass-paper-final.pdf>.
- Deb, K., A. Pratap, S. Agarwal, and T. Meyarivan. 2002. "A Fast and Elitist Multiobjective Genetic Algorithm: NSGA-II." *IEEE Transactions on Evolutionary Computation* 6 (2): 182–97. <https://doi.org/10.1109/4235.996017>.
- Duffie, John A., and William A Beckman. 2013. *Solar Engineering of Thermal Processes*. Hoboken, New Jersey: John Wiley & Sons. <https://doi.org/10.1002/9781118671603>.
- Evins, Ralph. 2013. "A Review of Computational Optimisation Methods Applied to Sustainable Building Design." *Renewable and Sustainable Energy Reviews* 22: 230–45. <https://doi.org/10.1016/j.rser.2013.02.004>.
- Galasiu, A, and C F Reinhart. 2007. "Current Daylighting Design Practice: A Survey." *Building Research and Information* 36 (2): 159–74.
- Galjaard, Salomé, Sander Hofman, and Shibo Ren. 2015. "Optimizing Structural Building Elements in Metal by Using Additive Manufacturing." In .
- Greenup, Phillip, Ian Edmonds, and Raphaël Compagnon. 2000. "RADIANCE Algorithm to Simulate Laser-Cut Panel Light-Redirecting Elements." *Lighting Research & Technology - LIGHTING RES TECHNOL* 32 (June): 49–54.
<https://doi.org/10.1177/096032710003200201>.
- Grobe, Lars O. 2019. "Photon Mapping in Image-Based Visual Comfort Assessments with BSDF Models of High Resolution." *Journal of Building Performance Simulation* 0 (0): 1–14. <https://doi.org/10.1080/19401493.2019.1653994>.
- Hemming-Xavier, Anja, and Markus Ostermaier. 2019. "3D Printing Innovation : New Facade Designed by Munich-Based Start-up 3F Studio for the Deutsches Museum Is the First of Its Kind Worldwide." Munich.
- "ImageNet, Large Scale Visual Recognition Challenge." 2017. 2017. <https://image-net.org/>.
- Imperiale, Alicia. 2018. "An ' Other ' Aesthetic : Moretti's Parametric Architecture." *Log*, no. 44: 71–82.
- Inamura, Chikara, Michael Stern, Daniel Lizardo, Peter Houk, and Neri Oxman. 2018. "Additive Manufacturing of Transparent Glass Structures." *3D Printing and Additive Manufacturing* 5 (4): 269–83. <https://doi.org/10.1089/3dp.2018.0157>.

- Inanici, Mehlika, and Jim Galvin. 2004. "Evaluation of High Dynamic Range Photography as a Luminance Mapping Technique." *Journal of Chemical Information and Modeling*. Vol. 53. Berkeley, CA. <https://doi.org/10.2172/841925>.
- Jakubiec, J. Alstan, and Christoph F. Reinhart. 2011. "DIVA 2.0: Integrating Daylight and Thermal Simulations Using Rhinoceros 3D, DAYSIM and EnergyPlus." *Proceedings of Building Simulation 2011: 12th Conference of International Building Performance Simulation Association*, 2202–9.
- Jakubiec, J A, and C F Reinhart. 2011. "DIVA-FOR-RHINO 2.0: Environmental Parametric Modeling in Rhinoceros/Grasshopper Using Radiance, Daysim and EnergyPlus." *Building Simulation 2011*. Sydney, Australia: IBPSA.
- Jiang, Caigui, Jun Wang, Philippe Bompas, Helmut Pottmann, and Johannes Wallner. 2013. "Freeform Shading and Lighting Systems from Planar Quads." *Rethinking Prototyping*, 335–46.
- Jipa, Andrei, Cristián Calvo Barentin, Gearóid Lydon, Matthias Rippmann, Georgia Chousou, Matteo Lomaglio, Arno Schlueter, Philippe Block, and Benjamin Dillenburger. 2019. "3D-Printed Formwork for Integrated Funicular Concrete Slabs." *Proceedings of the IASS Annual Symposium 2019 – Structural Membranes 2019*, no. October: 2019. <https://www.ingentaconnect.com/content/iass/piass/>.
- Jones, Nathaniel L., and Christoph F. Reinhart. 2017. "Experimental Validation of Ray Tracing as a Means of Image-Based Visual Discomfort Prediction." *Building and Environment* 113: 131–50. <https://doi.org/10.1016/j.buildenv.2016.08.023>.
- . 2019. "Effects of Real-Time Simulation Feedback on Design for Visual Comfort." *Journal of Building Performance Simulation* 12 (3): 343–61. <https://doi.org/10.1080/19401493.2018.1449889>.
- Kiser, Thomas, Michael Eigensatz, Minh Man Nguyen, Philippe Bompas, and Mark Pauly. 2012. "Architectural Caustics — Controlling Light with Geometry." In *Advances in Architectural Geometry 2012*, 91–106. Vienna: Springer Vienna. https://doi.org/10.1007/978-3-7091-1251-9_7.
- Klein, John, Michael Stern, Giorgia Franchin, Markus Kayser, Chikara Inamura, Shreya Dave, James C. Weaver, et al. 2015. "Additive Manufacturing of Optically Transparent Glass." *3D Printing and Additive Manufacturing* 2 (3): 92–105. <https://doi.org/10.1089/3dp.2015.0021>.

- Konis, Kyle, and Eleanor S. Lee. 2015. "Measured Daylighting Potential of a Static Optical Louver System under Real Sun and Sky Conditions." *Building and Environment* 92: 347–59. <https://doi.org/10.1016/j.buildenv.2015.04.024>.
- Lally, Sean. 2009. "New Material Boundaries." *Architectural Design* 79 (May/June).
- . 2014. *The Air From Other Planets A Brief History of Architecture to Come*. Lars Müller Publishers.
- LeCun, Yann, Bernhard Boser, John S Denker, Donnie Henderson, Richard E Howard, Wayne Hubbard, and Lawrence D Jackel. 1989. "Backpropagation Applied to Digit Recognition." *Neural Computation*.
- LUMA. 2017. *Jean Prouvé : Architect for Better Days*. London: Phaidon Press Limited.
- Manzan, Marco. 2014. "Genetic Optimization of External Fixed Shading Devices." *Energy & Buildings* 72: 431–40. <https://doi.org/10.1016/j.enbuild.2014.01.007>.
- Mardaljevic, J. 1995. "Validation of a Lighting Simulation Program under Real Sky Conditions." *Lighting Research & Technology* 27 (4): 181–88.
- Marsh, Andrew. 2003. "Computer-Optimized Shading Design." In *International, Eighth Conference, Ibpsa*, 831–38.
- Martin, Reinhold, and James Graham. 2016. "Climates : Architecture and the Planetary Imaginary." In *The Avery Review*, edited by James Graham, Caitlin Blanchfield, Alissa Anderson, Carver Jordan, and Jacob Moore. Lars Müller Publishers.
- McCue, Daniel. 2018. "JCHS Updated Household Growth Projections: 2018-2028 and 2028-2038." Cambridge, MA.
http://www.jchs.harvard.edu/sites/default/files/household_growth_projections2016_jchs.pdf.
- McNeel & Associates, Robert. 2020. "Rhino3d." 2020. <https://www.rhino3d.com>.
- McNeil, Andrew, and E. S. Lee. 2012. "A Validation of the Radiance Three-Phase Simulation Method for Modelling Annual Daylight Performance of Optically Complex Fenestration Systems." *Journal of Building Performance Simulation* 6 (1): 24–37. <https://doi.org/10.1080/19401493.2012.671852>.
- McNeil, Andrew, Eleanor S. Lee, and Jacob C. Jonsson. 2017. "Daylight Performance of a Microstructured Prismatic Window Film in Deep Open Plan Offices." *Building and Environment* 113: 280–97. <https://doi.org/10.1016/j.buildenv.2016.07.019>.

- Meibodi, Mania Aghaei, Andrei Jipa, Rena Giesecke, Demetris Shammass, Mathias Bernhard, Matthias Leschok, Konrad Graser, and Benjamin Dillenburger. 2018. "Smart Slab: Computational Design and Digital Fabrication of a Lightweight Concrete Slab." *Recalibration on Imprecision and Infidelity - Proceedings of the 38th Annual Conference of the Association for Computer Aided Design in Architecture, ACADIA 2018*, 434–43.
- Méndez, Tomás, Alfonso Capozzoli, Ylenia Cascone, and Mario Sassone. 2015. "The Early Design Stage of a Building Envelope : Multi-Objective Search through Heating , Cooling and Lighting Energy Performance Analysis" 154: 577–91.
<https://doi.org/10.1016/j.apenergy.2015.04.090>.
- Mueller, Caitlin T., and John A. Ochsendorf. 2015. "Combining Structural Performance and Designer Preferences in Evolutionary Design Space Exploration." *Automation in Construction* 52: 70–82. <https://doi.org/10.1016/j.autcon.2015.02.011>.
- NextEngine. 2020. "ScanStudioHD." 2020.
<http://www.nextengine.com/products/scanstudio-hd/>.
- Ochoa, Carlos E., Myriam B.C. Aries, and Jan L.M. Hensen. 2012. "State of the Art in Lighting Simulation for Building Science: A Literature Review." *Journal of Building Performance Simulation* 5 (4): 209–33.
<https://doi.org/10.1080/19401493.2011.558211>.
- Olgyay, Aladar, and Victor Olgyay. 1977. *Solar Control and Shading Devices*. Princeton NJ: Princeton University Press.
- Omidfar, Azadeh. 2011. "Design Optimization of a Contemporary High Performance Shading Screen- Integration of 'form' and Simulation Tools." *Proceedings of Building Simulation 2011: 12th Conference of International Building Performance Simulation Association*, no. January 2011: 2491–98.
- Papas, Marios, Thomas Houit, Derek Nowrouzezahrai, Markus Gross, and Wojciech Jarosz. 2012. "The Magic Lens: Refractive Steganography." *ACM Transactions on Graphics* 31 (6): 1–10. <https://doi.org/10.1145/2366145.2366205>.
- Papas, Marios, Wojciech Jarosz, Wenzel Jakob, Szymon Rusinkiewicz, Wojciech Matusik, and Tim Weyrich. 2011. "Goal-Based Caustics." In *Computer Graphics Forum*, 30:503–11. <https://doi.org/10.1111/j.1467-8659.2011.01876.x>.
- Perez, Richard, Robert Seals, and Joseph Michalsky. 1993. "All-Weather Model for Sky Lumina Nce Distribution - Preliminary Configuration and Validation." *Solar Energy* 50 (3): 235–45.

- Preisinger, Clemens, and Moritz Heimrath. 2014. "Karamba - A Toolkit for Parametric Structural Design." *Structural Engineering International: Journal of the International Association for Bridge and Structural Engineering (IABSE)* 24 (2): 217–21. <https://doi.org/10.2749/101686614X13830790993483>.
- Reindl, D T, W A Beckman, and J A Duffie. 1990. "Diffuse Fraction Correlations," no. I.
- Reinhart, C F, and M Andersen. 2006. "Development and Validation of a Radiance Model for a Translucent Panel." *Energy and Buildings* 38 (7): 890–904.
- Reinhart, C F, and O Walkenhorst. 2001. "Dynamic RADIANCE-Based Daylight Simulations for a Full-Scale Test Office with Outer Venetian Blinds." *Energy & Buildings* 33 (7): 683–97.
- Reinhart, Christoph. 2014. *Daylighting Handbook I Fundamentals, Designing with the Sun*. Cambridge.
- Rippmann, M., A. Liew, T. Van Mele, and P. Block. 2018. "Design, Fabrication and Testing of Discrete 3D Sand-Printed Floor Prototypes." *Materials Today Communications* 15 (June 2017): 254–59. <https://doi.org/10.1016/j.mtcomm.2018.03.005>.
- Ruffray, Nicolas, Mathias Bernhard, Andrei Jipa, Mania Meibodi, Neil de Taisne, Felix Stutz, Timothy Wangler, Robert Flatt, and Benjamin Dillenburger. 2017. "Complex Architectural Elements From Hpfrc and 3D Printed Sandstone." *RILEM Symposium on Ultra-High Performance Fibre-Reinforced Concrete* 1 (1): 135–44. [internal-pdf://68.86.147.16/UHPFRC2017_final_AJ_NR_TW.pdf](https://doi.org/10.1016/j.rilem.2017.06.005).
- Sadeghipour, Roudsari Mostapha, and Michelle Pak. 2013. "Ladybug: A Parametric Environmental Plugin for Grasshopper to Help Designers Create an Environmentally-Conscious Design." In *Proceedings of BS2013: 13th Conference of International Building Performance Simulation Association*. Chambery. https://www.ibpsa.org/proceedings/bs2013/p_2499.pdf.
- Sarat, Babu. 2018. "Betatype, Safran Electrical & Power, Customer Story."
- Saratsis, Emmanouil, Timur Dogan, and Christoph F Reinhart. 2017. "Simulation-Based Daylighting Analysis Procedure for Developing Urban Zoning Rules." *Building Research & Information* 45 (5): 478–91. <https://doi.org/10.1080/09613218.2016.1159850>.

- Sargent, Jon A., Jeffrey Niemasz, and Christoph F. Reinhart. 2011. "SHADERADE: Combining Rhinoceros and Energyplus for the Design of Static Exterior Shading Devices." *Proceedings of Building Simulation 2011: 12th Conference of International Building Performance Simulation Association*, 310–17.
- Schregle, Roland. 2003. "Bias Compensation for Photon Maps." *Computer Graphics Forum* 22 (4): 729–42. <https://doi.org/10.1111/j.1467-8659.2003.00720.x>.
- . 2004. "Daylight Simulation with Photon Maps." Saarland University.
- SideFX. 2020. "Houdini." <https://www.sidefx.com/>.
- Simonyan, Karen, and Andrew Zisserman. 2015. "Very Deep Convolutional Networks for Large-Scale Image Recognition." *3rd International Conference on Learning Representations, ICLR 2015 - Conference Track Proceedings*, 1–14.
- "The RADIANCE 5.1 Synthetic Imaging System." n.d. Accessed March 5, 2020. <https://floyd.lbl.gov/radiance/refer/ray.html>.
- Turrin, Michela, Peter Von Buelow, Axel Kilian, and Rudi Stouffs. 2012. "Automation in Construction Performative Skins for Passive Climatic Comfort A Parametric Design Process." *Automation in Construction* 22: 36–50. <https://doi.org/10.1016/j.autcon.2011.08.001>.
- Turrin, Michela, Peter Von Buelow, and Rudi Stouffs. 2011. "Design Explorations of Performance Driven Geometry in Architectural Design Using Parametric Modeling and Genetic Algorithms." *ADVANCED ENGINEERING INFORMATICS*. <https://doi.org/10.1016/j.aei.2011.07.009>.
- Vlachokostas, Alex, and Nicholas Madamopoulos. 2017. "Daylight and Thermal Harvesting Performance Evaluation of a Liquid Filled Prismatic Façade Using the Radiance Five-Phase Method and EnergyPlus." *Building and Environment* 126 (October): 396–409. <https://doi.org/10.1016/j.buildenv.2017.10.017>.
- Wang, J., C. Jiang, P. Bompas, J. Wallner, and H. Pottmann. 2013. "Discrete Line Congruences for Shading and Lighting Discrete Line Congruences for Shading and Lighting." In *Eurographics Symposium on Geometry Processing*. <https://doi.org/10.1111/cgf.12172>.
- Ward, G. and Shakespeare, R. 1998. *Rendering with Radiance: The Art and Science of Lighting Visualization*. Morgan Kaufman.

Woodward, Maggie. 2017. “Commercial Buildings Energy Consumption Survey (CBECS) Trends in Lighting in Commercial Buildings.” 2017.

<https://www.eia.gov/consumption/commercial/reports/2012/lighting/>.

World Green Building Council (WGBC), IEA, and UN-Environment. 2018. “2018 Global Status Report.”

https://webstore.iea.org/download/direct/2408?fileName=2018_Global_Status_Report.pdf.

Zhu, Jun Yan, Taesung Park, Phillip Isola, and Alexei A. Efros. 2017. “Unpaired Image-to-Image Translation Using Cycle-Consistent Adversarial Networks.” *Proceedings of the IEEE International Conference on Computer Vision* 2017-Octob: 2242–51.

<https://doi.org/10.1109/ICCV.2017.244>.

8 Appendix

8.1 Neural Net definitions

8.1.1 *NNI*

Layer (type)	Output Shape	Param #
conv2d_12 (Conv2D)	(None, 198, 198, 64)	640
activation_20 (Activation)	(None, 198, 198, 64)	0
max_pooling2d_12 (MaxPooling)	(None, 99, 99, 64)	0
conv2d_13 (Conv2D)	(None, 97, 97, 64)	36928
activation_21 (Activation)	(None, 97, 97, 64)	0
max_pooling2d_13 (MaxPooling)	(None, 48, 48, 64)	0
conv2d_14 (Conv2D)	(None, 46, 46, 64)	36928
activation_22 (Activation)	(None, 46, 46, 64)	0
max_pooling2d_14 (MaxPooling)	(None, 23, 23, 64)	0
flatten_4 (Flatten)	(None, 33856)	0
activation_23 (Activation)	(None, 33856)	0
dropout (Dropout)	(None, 33856)	0
dense_8 (Dense)	(None, 64)	2166848
activation_24 (Activation)	(None, 64)	0
dense_9 (Dense)	(None, 5)	325
Total params: 2,241,669		

loss: 0.0528

mean_absolute_error: 0.1729

mean_squared_error: 0.0453

8.1.2 NN2

Layer (type)	Output Shape	Param #
input_13 (InputLayer)	(None, 200, 200, 3)	0
block1_conv1 (Conv2D)	(None, 200, 200, 64)	1792
block1_conv2 (Conv2D)	(None, 200, 200, 64)	36928
block1_pool (MaxPooling2D)	(None, 100, 100, 64)	0
block2_conv1 (Conv2D)	(None, 100, 100, 128)	73856
block2_conv2 (Conv2D)	(None, 100, 100, 128)	147584
block2_pool (MaxPooling2D)	(None, 50, 50, 128)	0
block3_conv1 (Conv2D)	(None, 50, 50, 256)	295168
block3_conv2 (Conv2D)	(None, 50, 50, 256)	590080
block3_conv3 (Conv2D)	(None, 50, 50, 256)	590080
block3_pool (MaxPooling2D)	(None, 25, 25, 256)	0
block4_conv1 (Conv2D)	(None, 25, 25, 512)	1180160
block4_conv2 (Conv2D)	(None, 25, 25, 512)	2359808
block4_conv3 (Conv2D)	(None, 25, 25, 512)	2359808
block4_pool (MaxPooling2D)	(None, 12, 12, 512)	0
block5_conv1 (Conv2D)	(None, 12, 12, 512)	2359808
block5_conv2 (Conv2D)	(None, 12, 12, 512)	2359808
block5_conv3 (Conv2D)	(None, 12, 12, 512)	2359808
block5_pool (MaxPooling2D)	(None, 6, 6, 512)	0
flatten_9 (Flatten)	(None, 18432)	0
dense_17 (Dense)	(None, 1024)	18875392
dense_18 (Dense)	(None, 5)	5125
=====		
Total params: 33,595,205		
loss: 0.0453		
mean_absolute_error: 0.1560		
mean_squared_error: 0.0463		

8.1.3 NN3

Layer (type)	Output Shape	Param #
conv2d_11 (Conv2D)	(None, 197, 197, 4)	68
max_pooling2d_11 (MaxPooling)	(None, 98, 98, 4)	0
flatten_13 (Flatten)	(None, 38416)	0
dense_41 (Dense)	(None, 20)	768340
dense_42 (Dense)	(None, 10)	210
dense_43 (Dense)	(None, 5)	55
Total params: 768,673		

loss: 0.0460

mean_absolute_error: 0.1522

mean_squared_error: 0.0460